

**DIRECT INK WRITING OF ALUMINA THREE-
DIMENSIONAL STRUCTURES**

SOON MING SIANG

UNIVERSITI TUNKU ABDUL RAHMAN

**DIRECT INK WRITING OF ALUMINA THREE-DIMENSIONAL
STRUCTURES**

SOON MING SIANG

**A project report submitted in partial fulfilment of the
requirements for the award of Bachelor of Mechanical Engineering with
Honours**

**Lee Kong Chian Faculty of Engineering and Science
Universiti Tunku Abdul Rahman**

May 2023

DECLARATION

I hereby declare that this project report is based on my original work except for citations and quotations which have been duly acknowledged. I also declare that it has not been previously and concurrently submitted for any other degree or award at UTAR or other institutions.

Signature : 

Name : Soon Ming Siang

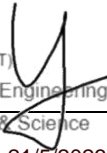
ID No. : 1804583

Date : 23 April 2023

APPROVAL FOR SUBMISSION

I certify that this project report entitled “**DIRECT INK WRITING OF ALUMINA THREE-DIMENSIONAL STRUCTURES**” was prepared by **SOON MING SIANG** has met the required standard for submission in partial fulfilment of the requirements for the award of Bachelor of Mechanical Engineering with Honours at Universiti Tunku Abdul Rahman.

Approved by,

Signature	:	Assoc. Prof. Ts. Dr. Yeo Wei Hong BEng (Hons), M Eng, PhD, CEng, MIET, P.Tech (MT) Department of Mechanical and Material Engineering Lee Kong Chian Faculty of Engineering & Science Universiti Tunku Abdul Rahman	 21/5/2023
Supervisor	:	<u>Ts. Dr. Yeo Wei Hong</u>	
Date	:	_____	
Signature	:	-	_____
Co-Supervisor	:	-	_____
Date	:	-	_____

The copyright of this report belongs to the author under the terms of the copyright Act 1987 as qualified by Intellectual Property Policy of Universiti Tunku Abdul Rahman. Due acknowledgement shall always be made of the use of any material contained in, or derived from, this report.

© 2023, Soon Ming Siang. All right reserved.

ABSTRACT

Currently, there is a research study of addition TiO_2 to alumina ceramic in the application of binder jet 3D printing but not yet in direct ink writing (DIW). Thus, our project tried to explore the possibility of adopting DIW method so that there will be more options to perform 3D printing of alumina ceramic. Addition of 1 wt% of TiO_2 was chosen as alumina ceramic doped with this amount of TiO_2 sintered under a lower temperature was found to be the most beneficial. TiO_2 can also be used as a sintering aids as it helps to lower down sintering temperature while resulting in high densification of the sintered printed structure. This project aims to investigate the effects of TiO_2 addition on the rheological properties of the alumina ink and the sinterability of the sintered printed part. Firstly, alumina powder was doped with TiO_2 powder through ball milling process. Next, cellulose acetate was dissolved in acetone and mixed with the powder mixture. The alumina slurry was loaded into syringes which loaded to a 3D printer to perform printing. The green part produced underwent thermal debinding and sintering processes and followed by the characterization tests. Another syringe loaded with alumina slurry was used to perform rheological tests. From the result, it was found that the addition of TiO_2 barely affect the particle size distribution and rheological result. But, from the result, it was noted that the surface area per gram, relative density, Vickers hardness value as well as volume shrinkage increased due to the TiO_2 . Thus, TiO_2 is such a good additive as it helps to lower down sintering temperature while improving the physical and mechanical properties of the sintered part and is proven workable in the application of the DIW technique.

TABLE OF CONTENTS

DECLARATION		i
APPROVAL FOR SUBMISSION		ii
ABSTRACT		iv
TABLE OF CONTENTS		v
LIST OF TABLES		vii
LIST OF FIGURES		viii
LIST OF SYMBOLS / ABBREVIATIONS		xi
 CHAPTER		
1	INTRODUCTION	1
	1.1 General Introduction	1
	1.2 Importance of the Study	2
	1.3 Problem Statement	2
	1.4 Aim and Objectives	3
	1.5 Scope and Limitation of the Study	3
	1.6 Contribution of the Study	4
	1.7 Outline of the Report	4
2	LITERATURE REVIEW	5
	2.1 Introduction	5
	2.2 3D Printing Technique	5
	2.3 Rheological Factors	7
	2.4 Ink Characteristics	12
	2.5 Printing Parameters	14
	2.6 Debinding Parameters	16
	2.7 Sintering Parameters	19
	2.8 Effect of TiO ₂ on the sinterability of 3D alumina structure	26
	2.9 Summary	27
3	METHODOLOGY AND WORK PLAN	28

3.1	Introduction	28
3.2	Workflow	28
3.3	Ink Preparation	29
	3.3.1 Powder Characteristics	31
	3.3.2 Rheology of the ink	31
	3.3.3 Slicer software	32
3.4	Debinding and Sintering Process	33
	3.4.1 Debinding profile	33
	3.4.2 Sintering profile	34
3.5	Characterization of Sintered Samples	35
	3.5.1 Scanning Electron Microscopy (SEM) Test	35
	3.5.2 X-Ray Diffraction (XRD) Test	35
	3.5.3 Thermal gravimetric analysis (TGA) Test	36
	3.5.4 Brunauer-Emmett-Teller (BET) Test	36
	3.5.5 Vickers Hardness Test	36
	3.5.6 Water Immersion Density Test	36
3.6	Analysis of alumina powder size	38
3.7	Summary	40
4	RESULTS AND DISCUSSION	41
	4.1 Particle Size Distribution Result	41
	4.2 Rheological Test Result	43
	4.3 Printing Result	48
	4.4 TGA Result	49
	4.5 SEM Result	50
	4.6 XRD Result	52
	4.7 Volume Shrinkage	52
	4.8 Water Immersion Density Test Result	53
	4.9 Vickers Hardness Test Result	54
5	CONCLUSIONS AND RECOMMENDATIONS	56
	5.1 Conclusions	56
	5.2 Recommendations for future work	57
	REFERENCES	59
	APPENDICES	65

LIST OF TABLES

Table 3.1:	Composition of the ink formulation.	31
Table 3.2:	Print setting inside PrusaSlicer.	33
Table 4.1:	Particle size distribution result for pure alumina powder and 1 wt% TiO ₂ doped alumina powder.	42

LIST OF FIGURES

Figure 2.1:	Schematic illustration of the Direct Ink Writing (DIW) technology.	7
Figure 2.2:	Flow Sweep Viscosity versus Shear Rate.	8
Figure 2.3:	Amplitude Sweep Test for Copper-Based Ink.	9
Figure 2.4:	Amplitude sweep test at a frequency of 1 Hz of a 30 wt.% Pluronic F127 hydrogel (a) and the same hydrogel loaded with 70 wt.% of β -TCP particles (b). Tests carried out at 23 C, using a 20 mm rough parallel plate geometry with a 500 μ m gap and a solvent trap.	10
Figure 2.5:	Relationship between G' , G'' and phase angle in a vector diagram.	11
Figure 2.6:	Frequency Sweep test for 5 wt% Copper-Based Ink.	11
Figure 2.7:	Result of 3ITT of a 30 wt.% Pluronic hydrogel (P30) and the same hydrogel loaded with β -TCP particles: 10 wt. % (P30-10), 30 wt. % (P30-30), 50 wt.% (P30-50) and 70 wt.% (P30-70).	12
Figure 2.8:	Diagram illustration of the cases of under-extrusion, optimal extrusion, over extrusion.	16
Figure 2.9:	Thermal Degradation Curve in Different Atmosphere.	18
Figure 2.10:	Temperature curves used for the debinding of the Al_2O_3 ceramics prepared through SLA.	18
Figure 2.11:	Dependence of the porosity on the heating rate for sintering at 1150 $^{\circ}C$ for 20 min.	20
Figure 2.12:	SEM images of alumina ceramics sintered at different temperatures: (a), (b) 1300 $^{\circ}C$, (c), (d) 1400 $^{\circ}C$, (e), (f) 1500 $^{\circ}C$ and (g), (h) 1600 $^{\circ}C$.	21
Figure 2.13:	The layered structure of sintered alumina ceramics observed by SEM: (A) 30 min; (B) 60 min; (C) 90 min; (D) 120 min; (E) 150 min; (F) 180 min.	22
Figure 2.14:	The interlayer spacing of the sintered alumina ceramics with different holding time.	22

Figure 2.15:	SEM image of alumina ceramics: (A) 30 min; (B) 60 min; (C) 90 min; (D) 120 min; (E) 150 min; (F) 180 min.	23
Figure 2.16:	Average grain size of sintered alumina ceramics with different holding time.	23
Figure 2.17:	Densification trend for alumina sintered in air and in fluoride atmosphere.	24
Figure 2.18:	Microstructure of alumina samples in air and in fluoride atmosphere.	25
Figure 2.19:	Sintering profile of alumina ceramic cores.	26
Figure 3.1:	Workflow of the project.	29
Figure 3.2:	Ball milling for the alumina powder and TiO ₂ powder.	30
Figure 3.3:	Equipment used for ink preparation. (a) Ultrasonic Cleaner. (b) Vacuum Desiccator.	30
Figure 3.4:	Alumina colloidal ink loaded into a syringe.	31
Figure 3.5:	Diagram of rheometer with parallel plate system.	32
Figure 3.6:	Debinding profile for this project.	34
Figure 3.7:	Sintering profile for this project.	35
Figure 3.8:	Diagram of the set up for water immersion density test.	37
Figure 3.9:	Sample to picture of alumina powder particle.	38
Figure 3.10:	MATLAB code for the conversion of the picture of alumina powder particle.	38
Figure 3.11:	Conversion to Black and white version via MATLAB code.	39
Figure 4.1:	Particle size distribution for pure alumina powder.	41
Figure 4.2:	Particle size distribution for 1 wt% TiO ₂ doped alumina powder.	41
Figure 4.3:	Flow curve result for the samples: (a) pure alumina ink. (b) 1wt% TiO ₂ doped alumina ink.	44
Figure 4.4:	Amplitude Sweep result for the samples: (a) pure alumina ink. (b) 1wt% TiO ₂ doped alumina ink.	46

Figure 4.5:	Frequency Sweep result for the samples: (a) pure alumina ink. (b) 1wt% TiO ₂ doped alumina ink.	47
Figure 4.6:	3ITT test result for the samples: (a) pure alumina ink. (b) 1wt% TiO ₂ doped alumina ink.	48
Figure 4.7:	Printing result of pure alumina green part with 40 vol% alumina content, 100 g/L binder concentration: (a) Sample 1. (b) Sample 2. (c) Sample 3. (d) Sample 4. (e) Sample 5.	49
Figure 4.8:	Printing result of 1 wt% TiO ₂ doped alumina green part with 40 vol% alumina content, 100 g/L binder concentration: (a) Sample 1. (b) Sample 2. (c) Sample 3. (d) Sample 4. (e) Sample 5.	49
Figure 4.9:	Weight percent versus temperature curve for pure alumina scrap (green part).	50
Figure 4.10:	SEM result for the samples: (a) pure alumina powder under 2k magnification (b) 1 wt% TiO ₂ doped alumina powder under 2k magnification. (c) pure alumina solid disk under 2k magnification. (d) pure alumina solid disk under 700 magnification. (e) 1wt% TiO ₂ doped alumina solid disk under 2k magnification (f) 1wt % TiO ₂ doped alumina solid disk under 700 magdnification.	51
Figure 4.11:	XRD peak pattern comparison between the samples: (a) pure alumina powder. (b) 1 wt% TiO ₂ doped alumina powder. (c) pure alumina solid disk. (d) 1 wt% TiO ₂ doped alumina solid disk.	52
Figure 4.12:	Volume Shrinkage comparison between pure alumina solid disk and 1 wt% TiO ₂ doped alumina solid disk.	53
Figure 4.13:	Relative Density Comparison between pure alumina solid disk and 1 wt% TiO ₂ doped alumina solid disk.	54
Figure 4.14:	Vickers Hardness value comparison between pure alumina solid disk and 1 wt% TiO ₂ doped alumina solid disk.	55

LIST OF SYMBOLS / ABBREVIATIONS

AM	Additive Manufacturing
SM	Subtractive manufacturing
SFF	Solid Freeform Fabrication
RP	Prototyping
DIW	Direct Ink Writing
PBF	Powder Bed Fusion
DED	Direct Energy Deposition
SLM	Selective Laser Melting
SEM	Scanning Electron Microscopy
XRD	X-Ray Diffraction
BET	Brunauer-Emmett-Teller
LVR	Linear viscoelastic range
PSD	Particle size distribution
TGA	Thermogravimetric analysis
YAG	Yttrium alumina garnet
G'	Storage modulus, Pa
G''	Loss modulus, Pa
τ	Shear Stress, Pa
τ_y	Yield Stress, Pa
K	Consistency Index, Pa·s ⁿ
$\dot{\gamma}$	Applied Shear Rate, s ⁻¹
n	Flow Index
ρ_a	Apparent density of test specimen in g/cm ³
ρ_b	Bulk density of test specimen in g/cm ³
m_1	Mass of dry test specimen in g
m_2	Apparent mass of immersed test specimen in g
m_3	Mass of soaked test specimen in g
ρ_L	Bulk density of liquid (distilled water), 0.997 in g/cm ³
v_{pore}	Volume of porosity in %
TiO ₂	Titanium Dioxide
3ITT	Three interval thixotropy test

LIST OF APPENDICES

NIL

CHAPTER 1

INTRODUCTION

1.1 General Introduction

Additive Manufacturing (AM) is a trendy technology nowadays that generates parts by layers from bottom to top. On the other hand, the subtractive manufacturing (SM) works by removing material to the desired shape (Linke, 2017), it is referred to those conventional manufacturing methods for which usually involves cutting processes like drilling, grinding, turning, milling and so on. AM recently is adopted by many people. This is because it helps to reduce waste and has a higher ability to produce more complex design compared to SM. These are the reasons why AM stands out among several manufacturing methods.

AM is often called Solid Freeform Fabrication (SFF), Rapid Prototyping (RP) or 3D Printing. The working principle of AM in fabricating parts is by generating layer-by-layer directly from 3D CAD model (M'Barki et al., 2017). Initially, the CAD model is converted into STL file which is then imported into slicer software to adjust the print setting like layer height, extrusion multiplier and print speed. Through this software, G-code is produced and is readable by the 3D printer. Therefore, the green body parts can be fabricated without any need of worker to in charge of and certain type of the 3D printing method have to undergo debinding and sintering process for the purpose of strengthening the internal structure of the fabricated parts.

In this project, the method adopted is Direct Ink Writing (DIW). Cellulose based binder with environmentally friendly micro porous (easily to be removed) behavior will be used together with acetone as well as the alumina powder with the specific composition to form the alumina paste. Next, a syringe containing alumina paste will be extruded and the ink deposit on the heating bed (not all DIW has to be equipped with heating bed) and the nozzle will follow a tool path that will be generated from the G-code via a STL file and thus creating the object layer by layer until the final dimension is printed completely. The green part produced needs further post-processing like debinding and sintering as the debinding process is to remove the binder while sintering process is to fuse particle bonding to stabilize the parts.

Although ceramic has been used extensively in the field of 3D printing, there are certain limitations when dealing with sophisticated geometry parts. The finished products tend to fracture due to their brittleness. Crack might develop inside the ceramics and reduce the surface finish and dimension of the products (Chen et al., 2019). Therefore, this problem has led us to explore more, expanding our raw material selection to alumina product.

1.2 Importance of the Study

This project is to find out the effect of the addition of Titanium Dioxide (TiO_2) to the alumina powder and that is workable and stable in the application of Direct Ink Writing (DIW) printing method in order to open up more options for the selection of material for this DIW method. The reason DIW method is used in the project is because it is much simpler to use, and it is cost-effective. There are some parameters related to the printability and the shape retainability after the extrusion to be studied along the way. Rheological tests will be carried out to exhibit the behavior of different compositions of Alumina colloidal ink to examine the rheological property of the ink. The green body must undergo post processing like sintering in order to study the physical and mechanical properties of the finished parts.

1.3 Problem Statement

There was a study carried out by Liu et al. (2023) regarding the addition of titanium dioxide (TiO_2) into cement-based material via binder jet 3D printing technique. They found out that TiO_2 able to improve the densification effect of the cement-based printed sample. The void inside the samples were filled by TiO_2 particles, making them more denser. Since there is already a research study of Titanium Dioxide in binder jet 3D printing but not yet in direct ink writing (DIW). Thus, our project comes into play by investigating the application of TiO_2 in alumina powder DIW technique since there is no research studying in this field currently.

Next, 1 wt% of TiO_2 was used in this project, this is because it is based on the research conducted by Ting et al. (2008). They found out that the sample doped with 1 wt% of TiO_2 sintered under 1450 °C was found to be the most effective and efficient throughout the studied range of TiO_2 . Not only that,

another research conducted by Li et al. (2017) proved that the secondary phase existed due to Al_2TiO_5 phase happened between 2 wt% and 5 wt% of TiO_2 -CuO content. The secondary phase reduces the Young's Modulus and thermal expansion coefficient of alumina matrix.

Normally the sintering temperature for ceramic alumina is between 1600 to 1700 °C. However, 1500 °C of sintering temperature was chosen due to the fact that TiO_2 able to act as a sintering aid to lower down the sintering temperature to 1500 °C. This is supported by the research carried out by Qian et al. (2023), proving that with the help of TiO_2 under 1500 °C sintering temperature, they managed to achieve a relative density of 95% for the sintered ceramics object using stereolithography technique. Since there is no research adopting the DIW technique, it is worth to explore the potential of performing 3D printing of alumina with the addition of TiO_2 via DIW method under the sintering temperature of 1500 °C.

1.4 Aim and Objectives

This project aims to investigating the effects of TiO_2 addition on the rheological properties of the alumina ink and the sinterability of the sintered printed part. The following are the detailed objectives of this project:

- a) To investigate the effect of addition of TiO_2 on the powder morphology of the alumina feedstock.
- b) To evaluate the rheological properties of the ink.
- c) To evaluate the physical and mechanical properties of the sintered structure.

1.5 Scope and Limitation of the Study

The scope of this study is primarily focused on the DIW for the optimal Alumina colloidal ink. Formulations of ink with and without the addition of 1 wt% of TiO_2 were prepared. Next, the samples were tested through 4 rheological test which are flow curve, amplitude sweep, and frequency sweep, and three interval thixotropy test (3ITT). The printability of the ink and shape retention were examined after printing. Debinding process was carried out to remove the binder by thermal degradation under the controlled temperature. Followed by sintering of debinded parts to strengthen the material and improve the integrity of the printed structure. And lastly, there 6 tests to study the characterization of the

sintered sample which are SEM, XRD, TGA, BET, Vickers Hardness Test as well as Water Immersion Density Test were carried out.

Whereas, for the limitation of the study, since there are many parameters such as printing speed, flow speed and so on in controlling the optimal condition for the printed parts and the rheological result. It is very hard to control all the parameters at once. In addition to that, there is no any universal standard exist to get the optimal value for each parameter. Throughout the whole test, the printing speed is set at 5 mm/s and flow speed is 100%. Therefore, many repetition of task has to be done which is quite time-consuming and impossible to achieve in the following FYP 2 repiod due to the lack of time.

1.6 Contribution of the Study

The pure alumina ink was doped with TiO_2 to investigate the effect on the rheological properties as well as the sinterability of the sintered part when compared to pure alumina ink. This research has found out that the addition of TiO_2 able to improve the distribution of particles, relative density as well as the hardness of the sintered samples. And there is no significant change in terms of the rheological properties, XRD result and printing quality when compared to the pure alumina ink.

1.7 Outline of the Report

The following chapter 2 is about the literature review on the 3D printing technique, rheological factors, ink characteristics, printing, debinding as well as sintering parameters. Next, chapter 3 is about the methodology on the ink preparation, debinding and sintering process, characterisation test, as well as the analysis of powder size of our raw material, alumina powder. Moreover, chapter 4 is the result and discussion part on the particle size distribution, rheology, TGA, SEM, XRD, volume shrinkage, water immersion density as well as Vickers Hardness tests. And will followed by chapter 5 which is the conclusions and recommendations for future work.

CHAPTER 2

LITERATURE REVIEW

2.1 Introduction

This section will describe the 3D Alumina Printing Technique in detail in section 2.2. The rheological factors that affect the printability of the ink will be explained in Section 2.3. The ink Characteristics are explained in Section 2.4. Printing parameters are crucial and things to take note of will be explained in Section 2.5. The thermal debinding and sintering process are explained in detail in Section 2.6 and Section 2.7. And a brief summary for this chapter 2 is made in Section 2.8.

2.2 3D Printing Technique

The exposure to 3D printing which is the additive manufacturing (AM) is getting bigger and this enlarges the scope of selecting type of raw material to ceramics. There is a breakthrough in the AM field with the advancement of technology, even the types of reliable metal alloys selected for printing is limited, there is still a good sign that help to solve the problem that those alloys processed in the conventional methods fail to print out the desired parts (Cooke et al., 2020). There are a few famous 3D printing methods which are Powder Bed Fusion (PBF) and Direct Energy Deposition (DED).

PBF utilizes a laser or an electron beam as a heating source to fuse or enhance the particle layer-by-layers until a solid and complete part is formed. A layer of powder is spread over the platform. A programmed tool path will be generated for the heating source to follow until the layer forms the desired 2D cross-section. Then, powder will be deposited on top using a roller, and the procedures are repeated until the final dimension of the part is achieved. The loose packed and unfused powder is to be removed in the post processing treatment process (Additive Manufacturing Research Group, n.d.). According to Sames et al. (2016), the post treatment process is needed to release the thermal residue stress that is accumulated during the sintering stage.

Direct Energy Deposition is another type of 3D printing technique that shares the same idea as in PBF which uses laser or electron beam to use the

powder. There is a supply of metal powder supplied through a nozzle onto a base and is melted when contact with the laser. The procedure is repeated until the part is solidified and completed. The electron-based system is performed in a vacuum environment to avoid the interaction of the electron with air particles. Whereas for laser-based application, it is done inside a chamber containing inert gas that is needed to prevent the metal from contamination (Sing et al., 2020). Similarly, post processing treatment is required to eliminate the thermal residue stress induced by the laser.

Both PBF and DED have the same problem that the deposited layer will sometimes partially re-melt and re-solidify and thus, forming columnar grains (Vilaro et al., 2011). This columnar grain is caused by steep thermal gradient and the uneven cooling of the solidified layers (Frazier, 2014). This grain also increases the thermal residue stress and distortion caused by the expansion and contraction within metal particles (Ding et al., 2015). Eventually, cracks and porosity might form and would lead to premature failure (Ngo et al., 2018).

The success of metal material in 3D printing has led the development of ceramics as a new form of material. Another method of 3D printing to be introduced here is the Direct Ink Writing (DIW) as this method is applied throughout the project. DIW is also known as Robocasting, it is extrusion-based technique utilizing a non-Newtonian viscous slurry as the printing ink at room temperature. The working principle of DIW is using a binder to hold all the ceramic powders together as a paste and then it is kept inside a syringe to be extruded out as a green part layer-by-layer under the room temperature condition (Bonada et al., 2019). The nozzle will be moved by the robotic arm based on the tool path generated from the SLT file and print the green part out in layer form. The green part will then undergo post-treatment processes such as debinding and sintering process to remove the binder and strengthen the particle bonding until the final part is obtained. The optimum rheological properties can be obtained through the selection of binder-to-ceramic ratio.

There are few advantages of using DIW throughout the project. First of all, the ink used in DIW is the ceramics slurry, due to its viscoelastic behavior, it provides a shape retention ability to the green part, therefore freestanding structure can be printed and it advantageous compared to other technique where support is needed while printing. Secondly, DIW is a simple, and less expensive

technique which do not require any involvement of laser or electron beam but able to have similar function as other method where the complex geometry able to be printed out with less defects. Lastly, DIW can performed under room temperature which avoid thermal and residue stresses from building up (Shahzad and Lazoglu, 2021). Figure 2.1 shows the schematic illustration of the Direct Ink Writing (DIW) technology.

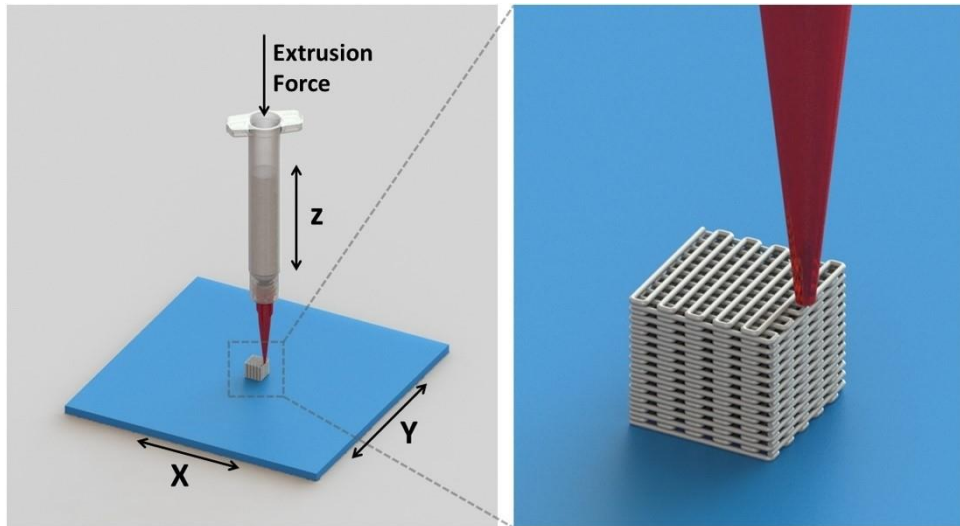


Figure 2.1: Schematic illustration of the Direct Ink Writing (DIW) technology (del-Mazo-Barbara and Ginebra, 2021).

2.3 Rheological Factors

Optimum rheological factors are crucial as they will affect the printability of the ink in the DIW method. The rheological properties that will determine the flowability and printability of the ink are viscosity, yield stress, viscoelasticity, and fast recovery of the elastic behavior right after the ink being extruded and all these factors will be monitored and examined using rheology tests (Tubío et al., 2018).

The viscosity can be analyzed from the graph of viscosity versus shear rate in the flow sweep test. The binder used is expected to be yield-pseudoplastic fluid and has shear thinning behavior. When the yield stress is exceeded, viscosity is expected to decrease when the shear rate increases, this behavior of the graph can be seen in Figure 2.2. Low viscosity reduces friction and thus allows the ink to flow. This is because low viscosity with lower shear rate has

higher flexibility in controlling the printing speed of the ink (Allaire et al., 1994).

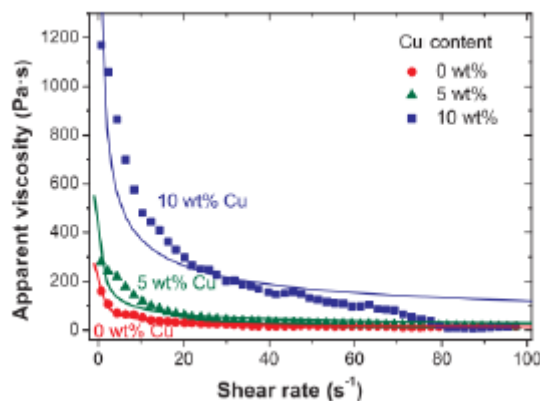


Figure 2.2: Flow Sweep Viscosity versus Shear Rate (Tubío et al., 2018).

The Hershel-Bulkley model can be used to illustrate how a non-Newtonian fluid is used in the DIW technique via equation 2.1. In the model, there are 3 assumptions which are, below yield point, an ink core is extruded under uniform speed, the outer yield shell is subjected to laminar flow, and there is slippage between the ink and inner wall of the nozzle (Smay et al., 2002). Therefore, a curve fitted is obtained from the viscosity graph due to the shear thinning behavior.

$$\tau = \tau_y + K \dot{\gamma}^n \quad (2.1)$$

where,

τ = Shear Stress in Pa

τ_y = Yield Stress in Pa

K = Consistency Index in Pa.sⁿ

$\dot{\gamma}$ = Applied Shear Rate in s⁻¹

n = Flow Index

The shape retention, flowability and sagging of the ink are heavily dependent on viscoelasticity and the yield point when the ink is extruded out from the nozzle. High yield strength is required in order to ensure support the stacking of layers (M'Barki et al., 2017). In the linear viscoelastic range (LVR)

region, the storage modulus is found to be fluctuated within a range before it decreases significantly when the yield strength is exceeded (Tubío et al., 2018). From there, it is noted that yield stress must be overcome in order to make the ink flow. Sagging is another issue where the green part is being pulled down by gravity before it solidifies. By having a high yield strength of the ink sagging can be solved and has higher shape retention ability after the ink is extruded through the nozzle (Rueschhoff et al., 2016). The amplitude sweep test is one of the dynamic oscillatory tests to find out the LVR, yield strength of the ink, by observing the drastic decrease in storage modulus which can be seen in Figure 2.3.

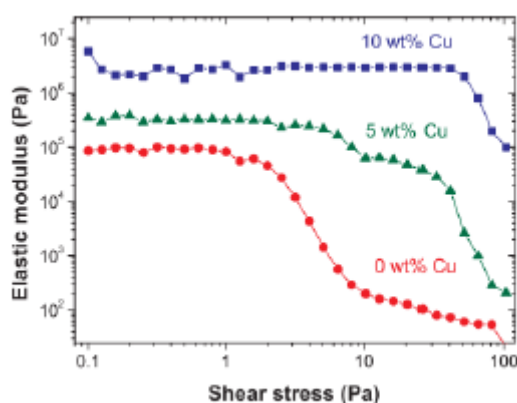


Figure 2.3: Amplitude Sweep Test for Copper-Based Ink (Tubío et al., 2018).

There is a study from del-Mazo-Barbara & Ginebra (2021) pertaining to the amplitude sweep test of different solid loading of hydrogel, referring to the figure 2.4, there are 3 obvious zone for both graphs. First zone is known as LVR, the storage modulus (G') is constant and larger than loss modulus (G''). G' at this zone is referring to elastic modulus at rest G'_{eq} . Point 1 represent yield point and the corresponding yield stress τ_y , which is the shear stress at the end of LVR region. The G' decreases signal the start of breaking down of internal structure, going into irreversible deformation. In second region, after the yield stress is exceeded G' still dominant over G'' . Point 2 represents the flow point. When $G' = G''$, this is the transition from solid-like behavior to liquid-like behavior. In third region, G'' finally dominant over G' , which means the material starts to flow.

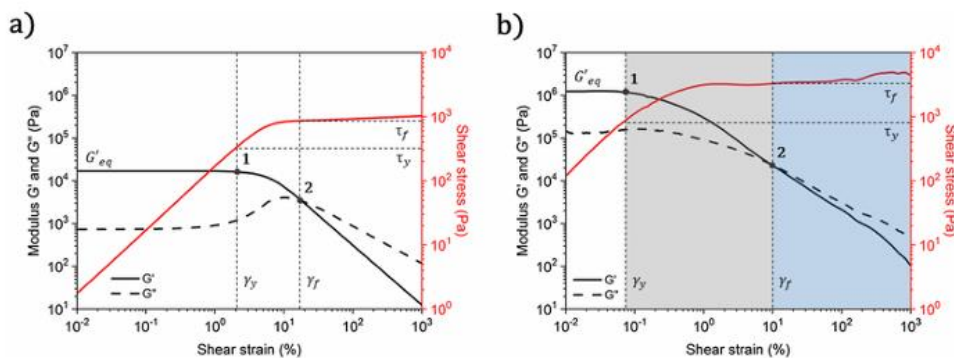


Figure 2.4: Amplitude sweep test at a frequency of 1 Hz of a 30 wt.% Pluronic F127 hydrogel (a) and the same hydrogel loaded with 70 wt.% of β -TCP particles (b). Tests carried out at 23 C, using a 20 mm rough parallel plate geometry with a 500 μ m gap and a solvent trap (del-Mazo-Barbara and Ginebra, 2021).

Next, viscoelasticity behavior can be represented by the storage modulus G' and loss modulus G'' where G' is the elastic or solid-like behavior and G'' is the viscous or liquid-like behavior (del-Mazo-Barbara and Ginebra, 2021). The higher storage modulus of the ink, the harder for it to flow. Besides, damping factor (tangent of phase angle) is the indication of viscoelastic dominancy. For example, perfect elastic behavior has a phase angle of 0° , which means there is no any viscous component. Whereas perfect viscous behavior has a phase angle of 90° , indicating that there is no any elastic component. Figure 2.5 shows the relationship between G' , G'' and phase angle where the y-axis is the viscous component and x-axis is the elastic component (del-Mazo-Barbara and Ginebra, 2021). For Frequency Sweep Test, the purpose of this test is to illustrate the viscoelasticity of the ink below yield strength within the LVR which can be seen in Figure 2.6 below.

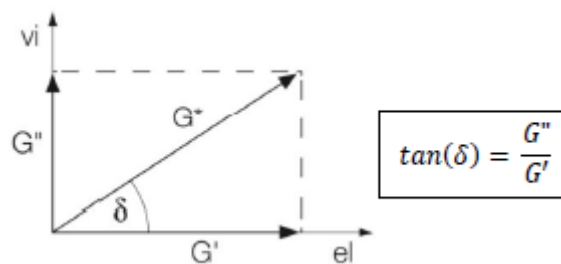


Figure 2.5: Relationship between G' , G'' and phase angle in a vector diagram (del-Mazo-Barbara and Ginebra, 2021).

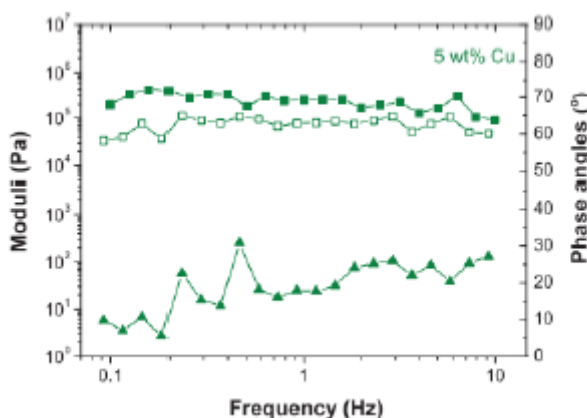


Figure 2.6: Frequency Sweep test for 5 wt% Copper-Based Ink (Tubío et al., 2018).

There is another test that measures the fast recovery of the elastic behavior of the ink in order to achieve good shape fidelity of the part which is three interval thixotropy (3ITT) test. The transition from fluid like to solid like is important to let the part has self-supporting ability after printing there are three intervals which are: first interval under very small shear rate refers to the ink at resting state while being extruded slowly, second interval under very high shear rate that refers to the extrusion of ink through small nozzle and lastly third interval under very small shear rate again refers to the resting state of the deposited ink. The ideal result is to get a high restored modulus to ensure good shape fidelity of the part. A study from del-Mazo-Barbara and Ginebra (2021) showed the result of 3ITT of the hydrogel ink with various ceramic contents which can be seen in Figure 2.7.

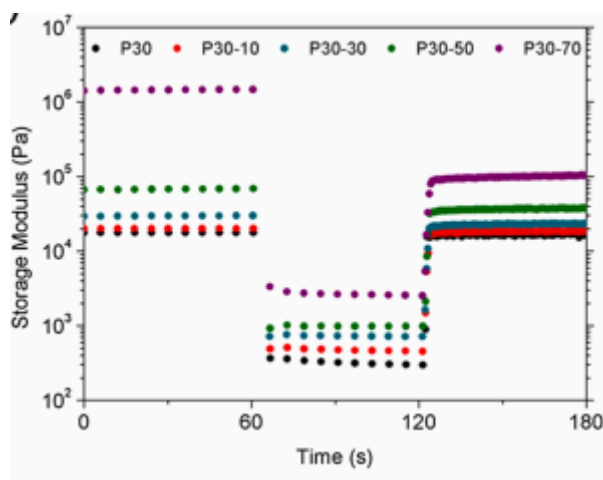


Figure 2.7: Result of 3ITT of a 30 wt.% Pluronic hydrogel (P30) and the same hydrogel loaded with β -TCP particles: 10 wt. % (P30-10), 30 wt. % (P30-30), 50 wt.% (P30-50) and 70 wt.% (P30-70) (del-Mazo-Barbara and Ginebra, 2021).

2.4 Ink Characteristics

Ink characteristics is important in controlling the rheological properties of the ink. There are a few of them which are binder concentration, additive, powder size, particle size distribution, powder shape and lastly mixing ratio. In this project, a binder is added to bind the powder particle together. The desired characteristics of the binder are to display a yield-pseudoplastic fluid and do not react with the mixture of the paste. And it will be removed in the later stage during debinding process.

First and foremost, binder concentration is closely linked to the yield and viscosity. When the binder concentration increases, then both the viscosity and the yield strength would increase as well. A study has proved that a 45 wt% concentration of Boehmite gel ink has higher viscosity than 43 wt% sample. The study is further supported by (M'Barki et al., 2017), showing that 45 wt% inks have higher elastic behavior. This is because higher concentration would lead to higher intermolecular interaction level between binder and the solvent in thus more bonding is formed between particles leading to increment in terms of strength. In overall, higher concentration of binder will increase the viscosity and hence reduce the flowability of the ink.

Furthermore, additives such as diethyl phthalate (a type of plasticizer) is to be added to increase yield strength and viscosity too (Godwin, 2000). Dispersant may be added as well to enhance the flowability by encouraging the binding of powder particles (Enneti et al., 2012). Not only that, but it also reduces the surface tension and increases the wettability of the ink making it more homogeneous and thus reduces the air bubble in the ink.

The packing density of the ink is dependent on the powder size, particle size distribution, and powder shape. Packing density is the degree of compactness of the particles and will give a big impact to the viscosity, porosity. Higher packing density means higher viscosity and higher yield strength. This is due to the increase in friction force between particles and an opposing force is exerted to prevent the part from deforming. Finer particle is more suitable as they can pack closely to each other and prevent formation of interstitial voids due to higher packing density. A study has been carried out by (Wu et al., 2016) to support this statement which is finer nano-sized alumina powder has higher density than micro-sized powder.

In addition, pores can be reduced when smaller size particle is used (Mostafaei et al., 2019). All these pores would cause defects and cracks which are vulnerable to the external force and lead to another problem during sintering process because the pores are unable to escape. Finer particles also have higher surface-to-volume ratio, and thus more surface is exposed and improving the densification (Yan et al., 2017).

Particle shape is also important as it will affect the packing density and flow characteristics. Spherical shaped particles have high packing density when compared to irregular shaped particles (Chateau, 2012). But, in terms of rheological properties, irregular shape particle has higher viscosity and yield strength due to the higher frictional support it holds in certain direction. However, the uneven friction in direction would lead to high anisotropic shrinkage after sintering process. Although spherical particles have lower viscosity and yield strength, they only have smaller distortion during sintering process in the aspect of defect formation and shrinkage. It can be solved by changing the size of the spherical particle which is quite similar to the concept of having irregular shape particle (Enneti et al., 2012).

For the particle size distribution (PSD), it refers to the suspension of different powder sizes within a fluid. The common categories such as D10, D50 and D90. For example, D10 refers to 10% of the particles are smaller than the specified particle size and 90% of the particles are larger than that. There is a study claimed that a wider PSD is able to reach the highest densification and lowest porosity (Mostafaei et al., 2019). This is due to a wider PSD having smaller particles able to fill the gaps between larger particles thus reduces pore and improving densification of the parts (Sahari et al., 2016).

Last but not least, the mixing ratio between filler powder and binder could affect the solid loading too. It indicates the solid filler to liquid binder content. Higher solid loading means having a large number of powder and will increase the viscosity. Viscosity is affected by filler content more significantly (Sahari et al., 2016). This is because of higher interparticle friction due to more collisions between particles. This statement is supported by (Supati et al., 2000) where higher solid loading is proven to have higher viscosity.

However, there is excess solid loading, the binder is not enough to fill the gaps between particles, thus formation of pores will occur and weaken the strength of the green part produced. On the other hand, when solid loading is insufficient, it will increase flowability of the ink as the viscosity decreases, thus the ink is easier to be extruded. In the case when there is excess of binder volume fraction, this will reduce the yield strength and shape retention ability. Large volume shrinkage will happen during debinding and sintering processes as the distance between particles increases. This statement is supported by Li et al. (2007) when a study conducted by the authors proven that 72 wt% powder loading (excess solid loading) has lower rheological performance than the solid loadings lower than 68 wt% which are the case of excess binder. All in all, solid loading has to be optimized to prevent shrinkage during debinding and sintering processes.

2.5 Printing Parameters

There are few printing parameters that can affect the printability of the ink. By optimizing these printing parameters, the qualities of the printing which are surface finish, dimension, resolution, drying period, printing time, and porosity of the ink can be controlled. Printing parameters such as nozzle diameter,

printing speed, layer thickness and extrusion rate must be adjusted to the optimum value in order to produce a high quality of green part.

In the project, smaller green parts with its geometrical detail are to be printed, therefore, printing resolution plays an important role in surface finish of the green parts. Printing resolution depends on the size of nozzle used, small nozzle size will result in high resolution of the green body as the ink extruded out from the nozzle is thinner. According to Feilden et al. (2016), when a large nozzle is used, the dimensional accuracy effect is poor. In addition, when the surface finish is in low quality, this is mostly due to the formation of cracks. This is because, when the surface finish of the part is poor, there will be a weaker region that is vulnerable and potentially forms the cracks.

The diameter of the ink is also very important as it may cause porosity in the green body. The larger the diameter of the ink decreases the surface-to-volume ratio, the lesser the surface is contacted with air and hence reduces the drying rate and promotes more porosities formation. This is due to the slow drying rate of the inner layer of the ink when the outer layer is evaporated first as it is directly contacted with air. This is a serious issue as the inner layer is still wet and the air is trapped because the air bubble cannot escape out due to the high drying rate of outer wall and thus leading to the formation of porosity.

Extrusion rate is a measure of the amount of ink that is extruded out per time. It must be controlled well because when it is too high, it will cause over-extrusion. Not only that, high extrusion rate will induce porosity formation also as the layers do not overlap fitly. On the other hand, when extrusion rate is too low, ink will not be extruded out sufficiently and lead to under-extrusion case. Sometimes, clogging of the ink might occur and stop the whole printing process. Therefore, extrusion rate has a direct impact on the print quality of the 3d printed part. Figure 2.8 showed the diagram illustration of the cases of under-extrusion, optimal extrusion and over-extrusion.

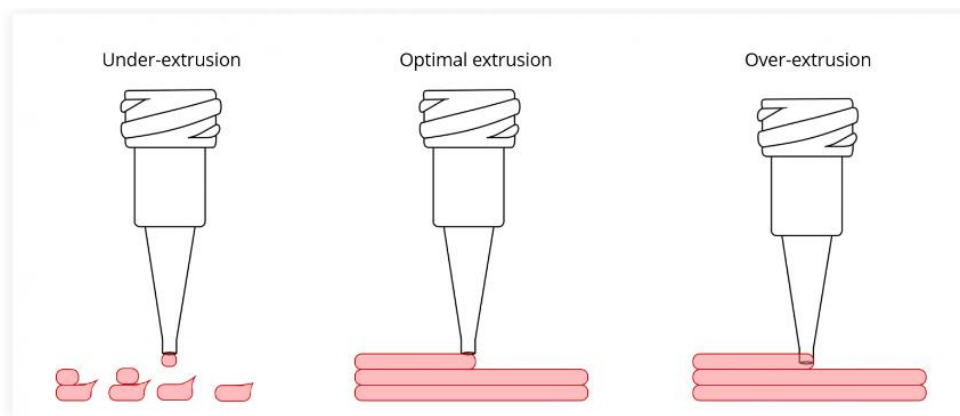


Figure 2.8: Diagram illustration of the cases of under-extrusion, optimal extrusion, over extrusion (Support, 2020).

Dimensional accuracy is a very crucial criterion when smaller and finer parts are required to be printed where only low tolerance of the dimension is given. Except nozzle diameter or size, printing speed and layers thickness are equally important to give an excellent dimensional accuracy. When printing speed is higher, the period for the printing process is reduced. But high printing speed also will cause the change in the sharp corner where it should be rounded (Feilden et al., 2016). Plus, high printing speed will lead to inconsistent extrusion width, so the ink cannot be deposited on the layers and there is also a buildup pressure issue in the syringe extrusion system that will affect the quality of the printing.

When thickness of layer is kept low, the ink will dry quicker which helps to solve the differential drying rate of the inner and outer layer of the ink and reduce the formation of porosity. But there is a compromise needed when setting the value for the thickness of layer as it might cause clogging of the ink.

2.6 Debinding Parameters

Through this DIW technique, a binder will be used to bind the alumina powder. After the green part is produced, it has to undergo a process called debinding process to remove the binder and the part is then called a brown part. The binder removal is done via thermal degradation hopefully to burn off all carbon content. However, most of the binder would retain some carbon content that that is not desired when moving on to sintering process. There are few debinding parameters to be discussed here such as debinding temperature, heating rate and

debinding environment, so that the carbon residue can be eliminated as much as possible before entering the sintering process.

The technique used in this project for debinding is thermal debinding. The binder will depolymerize to the state where it becomes volatile and will break down at high temperature. The debinding temperature must be high enough to ensure the binders debind completely. Supriadi et al. (2017) showed that increase in mass reduction has been recorded when the holding time prolonged in a slow heating rate. The slow heating rate enables the binder to be removed slowly, temperature gradient is minimized, and cause little cracks during the debinding process (Tafti et al., 2021). Hence, the slowest heating rate is desired in order to ensure the quality of the print.

Debinding environment is also a factor that could affect the carbon residue left within the brown part. In ambient air, in most cases, it will have a better removal effect of binder. This is due to the reaction of carbon with oxygen and thus the product formed, carbon dioxide, is released into the atmosphere. A study shows the different thermogravimetric analysis (TGA) result in different environments which are in nitrogen gas and in air (Lucena et al., 2003). The study proved that the degradation of binder in air condition resulted in less carbon content left compared to that of the nitrogen gas condition as seen in figure 2.9. TGA can determine the material's thermal stability and its volatile component by keeping track of the change of mass of the part when the temperature changes at a constant rate. when there is no change of mass in the specific range of temperature, then at this moment, it is described as thermally stable which helps to identify the suitable debinding temperature.

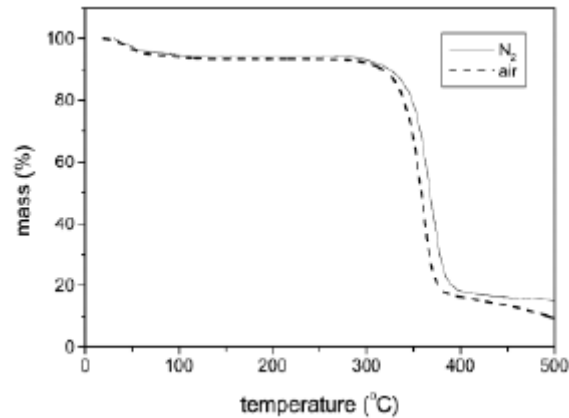


Figure 2.9: Thermal Degradation Curve in Different Atmosphere (Lucena et al., 2003).

In addition, there is a study from Wu et al. (2016) showed that vacuum debinding and traditional thermal debinding are carried out for the sample of alumina ceramics by Stereolithography (SLA) 3d printing technique. The vacuum debinding is conducted in a tube furnace while the thermal debinding is carried out in a traditional furnace. The debinding profiles are shown in figure 2.10. The result also showed that vacuum debinding will cause the sample to have much higher relative density compared to thermal debinding. The premixed solution to be used a binder consist of acrylamide, methylenebisacrylamide, glycerine and deionized water.

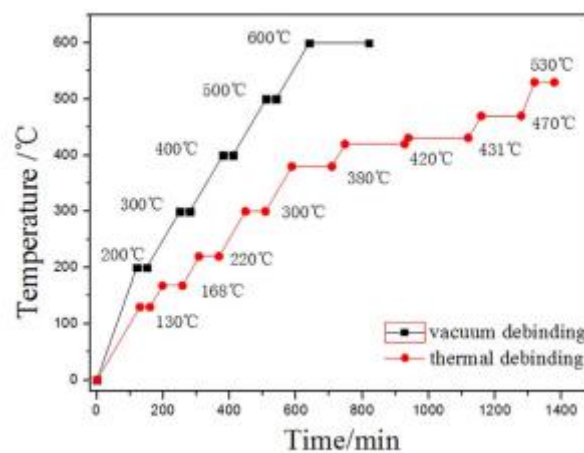


Figure 2.10: Temperature curves used for the debinding of the Al₂O₃ ceramics prepared through SLA (Wu et al., 2016).

2.7 Sintering Parameters

After debinding process, the brown part will proceed to the last stage, which is sintering process in order to complete the whole DIW technique throughout this project. Ideally, the remaining carbon residue within the brown part is to be removed during sintering process at a higher temperature, below the melting point of the alumina which is at 1600 °C. This higher temperature also helps to fuse the particle together to improve their structure integrity by forming bonds and fill up the remaining void from debinding process (Heaney, 2012). The sintering process promotes densification of particles. the adjacent particles will fuse together first starting from the formation of necks and grow further to form bridges that allow the atom will diffuse across by surface transport mechanism and further thickening the necks (Heaney, 2012). At the same time, the voids will be occupied. However, there would be a minor shrinkage due to the increase in density without any addition of the particles. Therefore, dimensional tolerance must be set.

There are few sintering parameters such as heating rate, sintering temperature, holding time and sintering environment to be optimized in order to obtain a high quality of printing. During heating of the brown part, due to Kirkendall effect, the different diffusion coefficient between 2 materials promote diffusion to take place. Thus, the diffusion of atom lead to the formation of pore (Gupta et al., 2018).

In terms of porosity, when the heating rate is low, fine pores will remain while heating rate is high, lot of bigger pores are observed which can be seen in figure 2.11. Theoretically, smaller grain size refers to larger grain boundary area that is under the low heating rate condition may improve the rate of diffusion across the boundary area and subsequently enhance densification. In addition to that, smaller grain size also helps to reduce the flow stress along the grain boundary too (Kim et al., 2009).

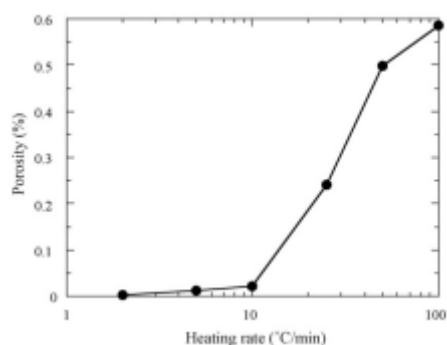


Figure 2.11: Dependence of the porosity on the heating rate for sintering at 1150 °C for 20 min (Kim et al., 2009).

The rate of diffusion increases with the rate of swelling. Lower heating rate will cause more swelling. On the other hand, when a higher heating rate is used, leading to more liquid formation. Generally, swelling is caused by the temperature where the liquid formation is induced (Gupta et al., 2018). Although higher heating rate can obtain finer microstructure, but the uneven densification will occur can result in non-uniform microstructure.

There is a study from Liu et al. (2022), which showed the effect of different sintering temperature on the morphology of alumina ceramic grain which can be seen in figure 2.12. It is noted that when the sintering temperature increases to a suitable range, the growth and order of alumina grain will be improved. When sintering temperature is 1500 °C, the grain distribution is more evenly distributed as the pores and void are reduced due to the high solid phase diffusion mass transfer rate at high temperature, therefore the densification effect is getting better. However, when temperature increases further, there is unusual grain growth, thereby reducing the mechanical properties of alumina ceramics.

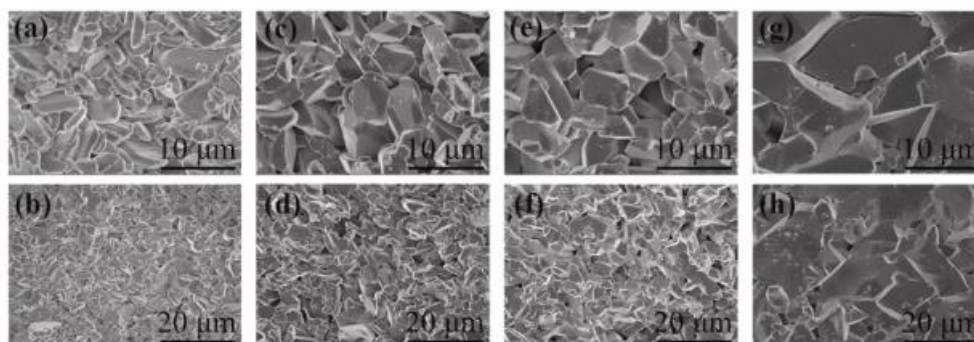


Figure 2.12: SEM images of alumina ceramics sintered at different temperatures: (a), (b) 1300 °C, (c), (d) 1400 °C, (e), (f) 1500 °C and (g), (h) 1600 °C (Liu et al., 2022).

Next, holding time plays an important role to ensure the quality of printing during sintering. A study showed that the alumina ceramics are sintered by different holding time, and the results are recorded. From Figure 2.13, cracks with 4.1 micron in size are found when the holding time is 30 minutes, but when increasing to 60 minutes and above, there is no any crack formation. From here, it is believed that longer holding time helps to reduce the formation of cracks as high holding time provides more time for the particle to grow and reduce the void in between the particle boundaries, hence cracks are reduced. Another result is noted that when holding time increases, the interlayer spacing will decrease which can be seen in Figure 2.14 as the holding time is 30 minutes the interlayer spacing is 24.7 micron while the holding time is 180 minutes, the interlayer spacing is 8.4 micron. In addition, from Figure 2.15, it showed that when holding time is 30 minutes, pore with 6.0 micron is formed and when the time increased to 60 minutes, the pore size reduces to 4.1 micron, and lastly when the time is increased further to 90 minutes and above, no more pores are formed. From there, it is noted that longer holding time could reduce the pore formation. In terms of average grain size, the study also studied that when the holding time increases, the average grain size will increase and stay approximately constant when the holding time is more than 120 minutes which can be seen from Figure 2.16. Therefore, 120 minutes is considered suitable as there is no significant increase in the grain size (Pan et al., 2020).

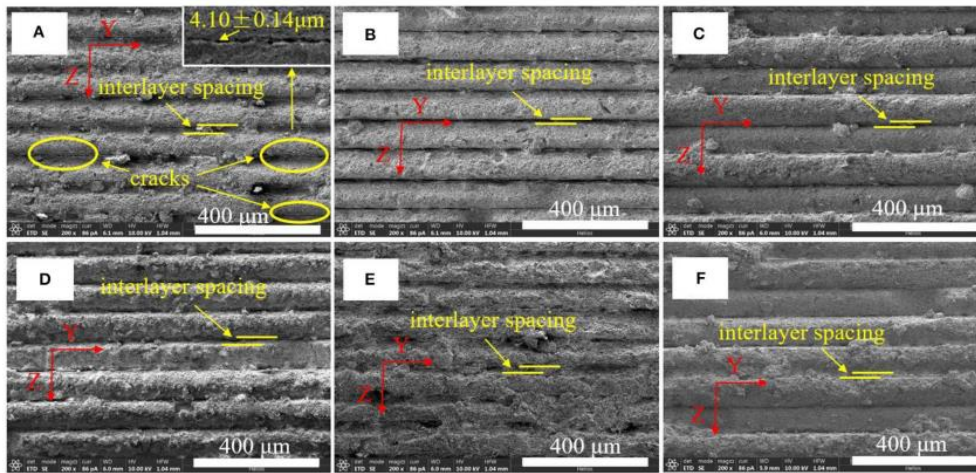


Figure 2.13: The layered structure of sintered alumina ceramics observed by SEM: (A) 30 min; (B) 60 min; (C) 90 min; (D) 120 min; (E) 150 min; (F) 180 min (Pan et al., 2020).

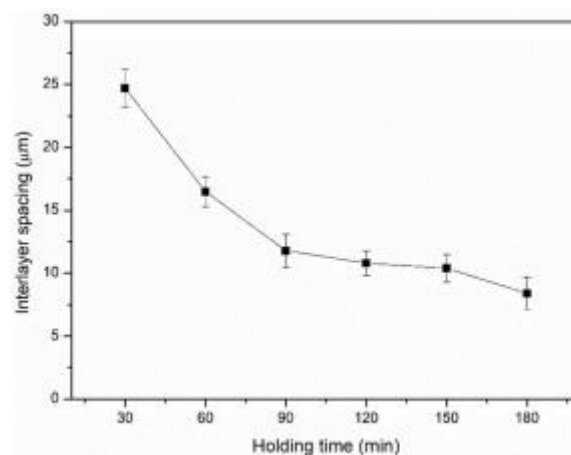


Figure 2.14: The interlayer spacing of the sintered alumina ceramics with different holding time (Pan et al., 2020).

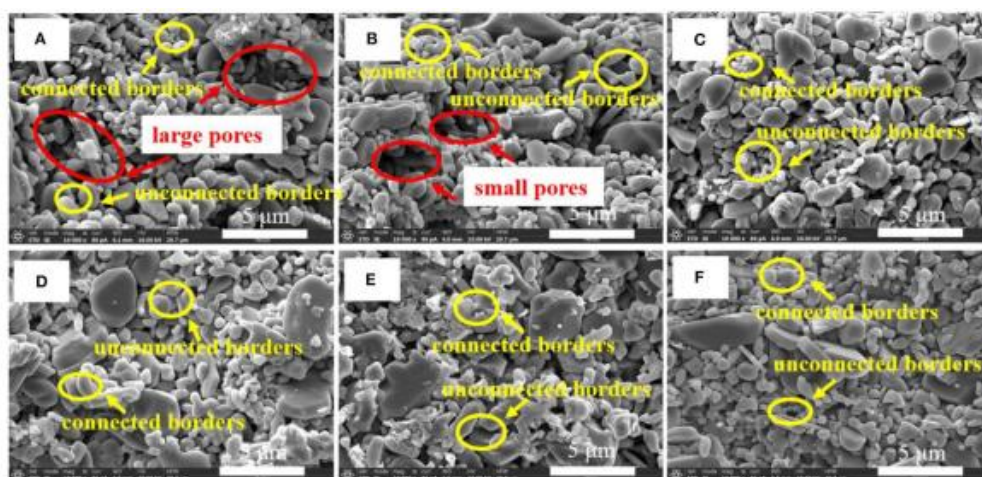


Figure 2.15: SEM image of alumina ceramics: (A) 30 min; (B) 60 min; (C) 90 min; (D) 120 min; (E) 150 min; (F) 180 min (Pan et al., 2020).

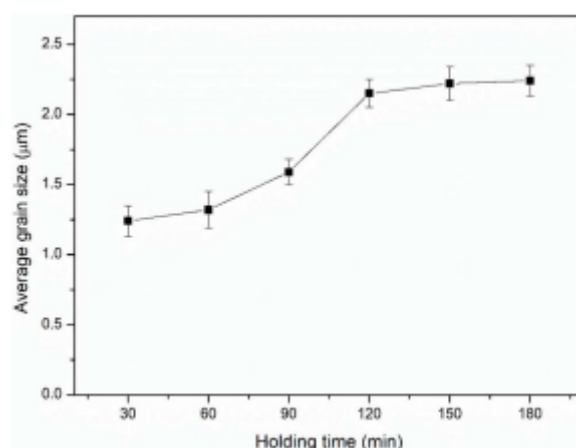


Figure 2.16: Average grain size of sintered alumina ceramics with different holding time (Pan et al., 2020).

Last but not least, sintering environment is also very crucial to obtain a good quality of sintered part. There is a study from Roy (1995), which showed the effect of densification of alumina in air and fluoride atmosphere. The result of the study is that the densification effect of alumina in air is better as it reached $3.8 \text{ gm}\cdot\text{cm}^{-3}$ which was 35% higher compared to fluoride atmosphere which can be seen from Figure 2.17. In terms of microstructure, it can be seen from Figure 2.18, the fluoride atmosphere helps to develop large grains while in air, it can be noticed that the neck growth and interconnected grains with the porosity. Fracture will take place in the fluoride atmosphere via grain boundaries due to the presence of the grains are parallel to the place of

micrograph which direct toward the grain boundary region. It also can be noted from the fluoride atmosphere, there are formation of large grains and intergranular porosity. The fast growth rate of the grain indicates that the high mobility for the grain boundary, at the same time the pore mobility will increase as well since the pores are not embedded inside the grains. Thus, the formation of aluminium fluoride can lead to volatilization. Plus, the partial pressure of the fluorides can induce mass transport via vapor phase and further increase pore mobility which will inhibit the densification of alumina. However, the possible reaction among fluoride, oxyfluoride, oxide and other impurities could form a range of low melting phase, and when the ionic diffusion is increase in a faster rate, it favors the densification effect All in all, fluoride atmospheric sintering is dependent on temperature because it can act as a helper or an inhibitor to densification of the alumina.

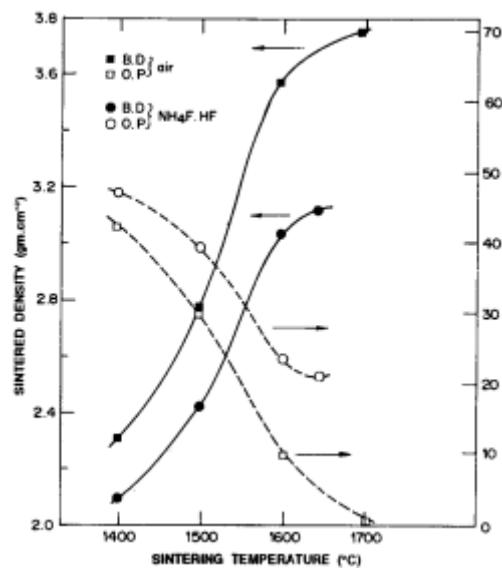


Figure 2.17: Densification trend for alumina sintered in air and in fluoride atmosphere (Roy, 1995).

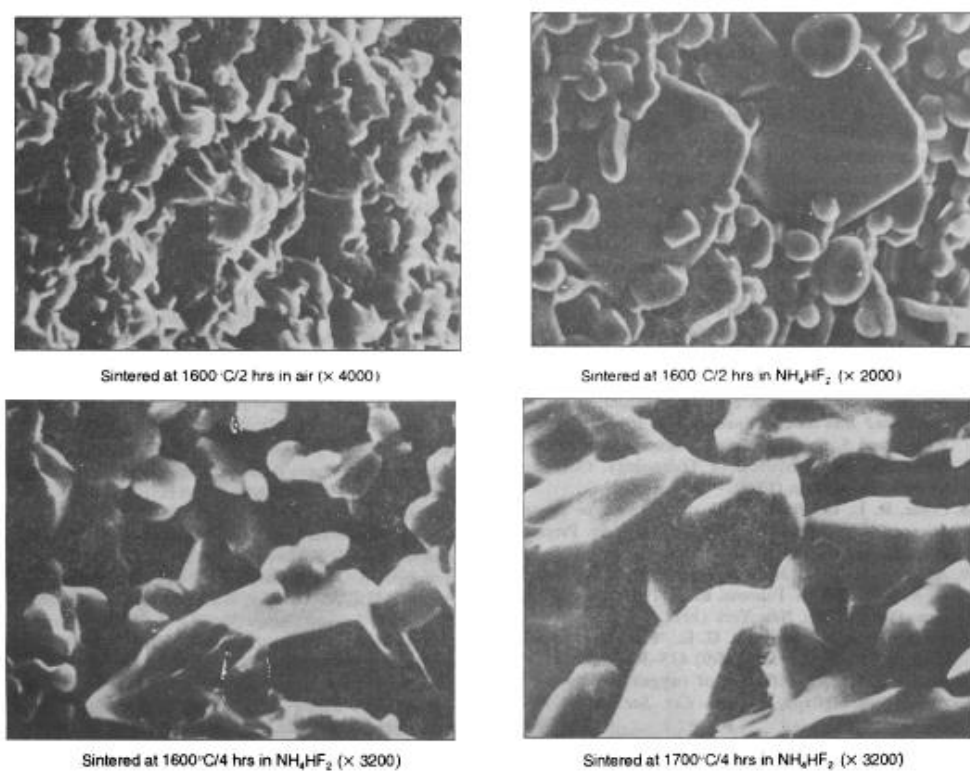


Figure 2.18: Microstructure of alumina samples in air and in fluoride atmosphere (Roy, 1995).

Lastly, a study is carried out to examine the alumina ceramic cores. For the sintering process, it is followed by the sintering profile as shown in figure 2.19 in the argon atmosphere. The samples are transferred to a tube furnace, and the temperature is increased to 200 °C with heating rate of 2 °C/min. After that the sample is heated to 550 °C with heating rate of 1 °C/min and retain the temperature for 2 hours and then is heated again to the targeted temperature as shown in the same figure with heating rate of 5 °C/min and maintained for 2 hours. The samples are then cooled to 600 °C with heating rate of 5 °C/min and is proceeded to furnace cooling (Li et al., 2020).

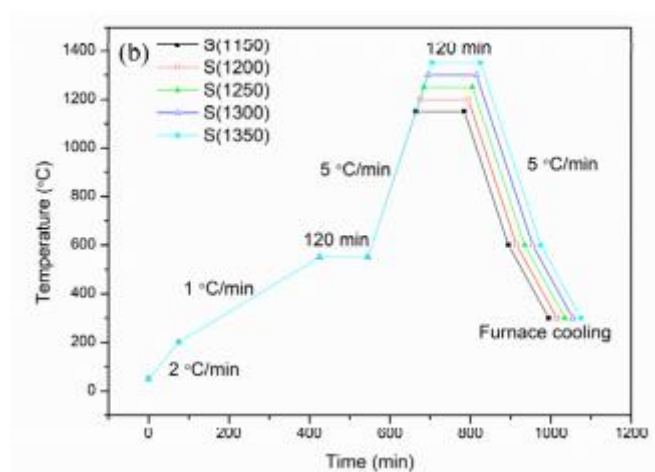


Figure 2.19: Sintering profile of alumina ceramic cores (Li et al., 2020).

2.8 Effect of TiO₂ on the sinterability of 3D alumina structure

There is a study conducted by Liu et al. (2023) by applying the Titanium Dioxide (TiO₂) into cement-based material via binder jet 3D printing technique. They found out that due to the addition of TiO₂ into their material, cement-based material, making the filling and nucleation effect more efficient in the material. Therefore, the relative density of the samples improved by quite a large amount due to the smaller size of TiO₂, filling the voids inside the printed samples. This indicated that the additive, TiO₂ helps in improving the relative density of the material. However, currently there is no any research studying on the application of TiO₂ in alumina ceramic via Direct Ink Writing (DIW) technique. Therefore, this project aims to investigate the effect of the TiO₂ on the 3d printing of alumina using DIW method.

There is also a study carried out by Ting et al. (2008) to support the addition of TiO₂ into alumina ceramic. They found out that under the constant sintering temperature at 1400 °C and 1450 °C, the increase in weight percent of TiO₂ helped to improve the bulk density of alumina ceramic but for 1600 °C, there is no significant effect when the weight percent increases. Therefore, it can be concluded that the addition of TiO₂ able to lower down the sintering temperature while maintaining the trend which is when weight percent of TiO₂ increases, the bulk density of the sintered alumina sample increases too.

2.9 Summary

In summary, chapter 2 discusses the 3D printing technique which includes the famous printing method, PBF and DED. The method used in this project is DIW and the reason is further explained in the subsection. Not only that, but rheological factors also that have the direct impact towards printability of the ink such as viscosity, yield stress viscoelastic properties are explained in detail. Moreover, ink characteristics such as binder concentration, additive, powder size, particle size distribution, powder shape and mixing ratio is described in detail as well. Furthermore, the relationship between printing parameters such as nozzle diameter, printing speed, layer thickness and extrusion rate quality of the green parts are explained with many supporting details. Last but not least, debinding and sintering parameters, for instance, heating rate, debinding and sintering environment, and temperature and sintering time will be discussed in detail. Lastly, the effect of TiO_2 on the sinterability of 3D alumina structure is discussed and explained in details by introducing addition of TiO_2 to cement-based material to perform binder jet 3D printing technique as well as the addition of TiO_2 helps to improve the bulk density of alumina ceramic when the weight percent of TiO_2 increases.

CHAPTER 3

METHODOLOGY AND WORK PLAN

3.1 Introduction

This section describes the procedure for carrying out this project in detail. The workflow for the overall project is shown clearly in Section 3.2. The ink preparation, powder characterization and rheology of the ink are explained in Section 3.3. The thermal debinding and sintering process about the debinding curve and sintering profile are explained in Section 3.4. Characterization of Sintered Samples through several tests are explained in Section 3.5. Analysis of alumina powder size is explained in section 3.6. And a brief summary for this chapter 3 is made in Section 3.7.

3.2 Workflow

Figure 3.1 shows the workflow for this project. Sample preparation was introduced by doping the alumina powder with TiO_2 powder through ball milling process and followed by rheology test for the ink to investigate the effect of the addition of TiO_2 to the raw material, alumina powder. Next, 3D printing was carried out to examine the printability and shape retention of the green part. Those green part underwent thermal debinding and sintering and performance of the sintered part was examined through characterization tests, data obtained from the characterization test regarding the physical and mechanical property of the sintered parts were analyzed.

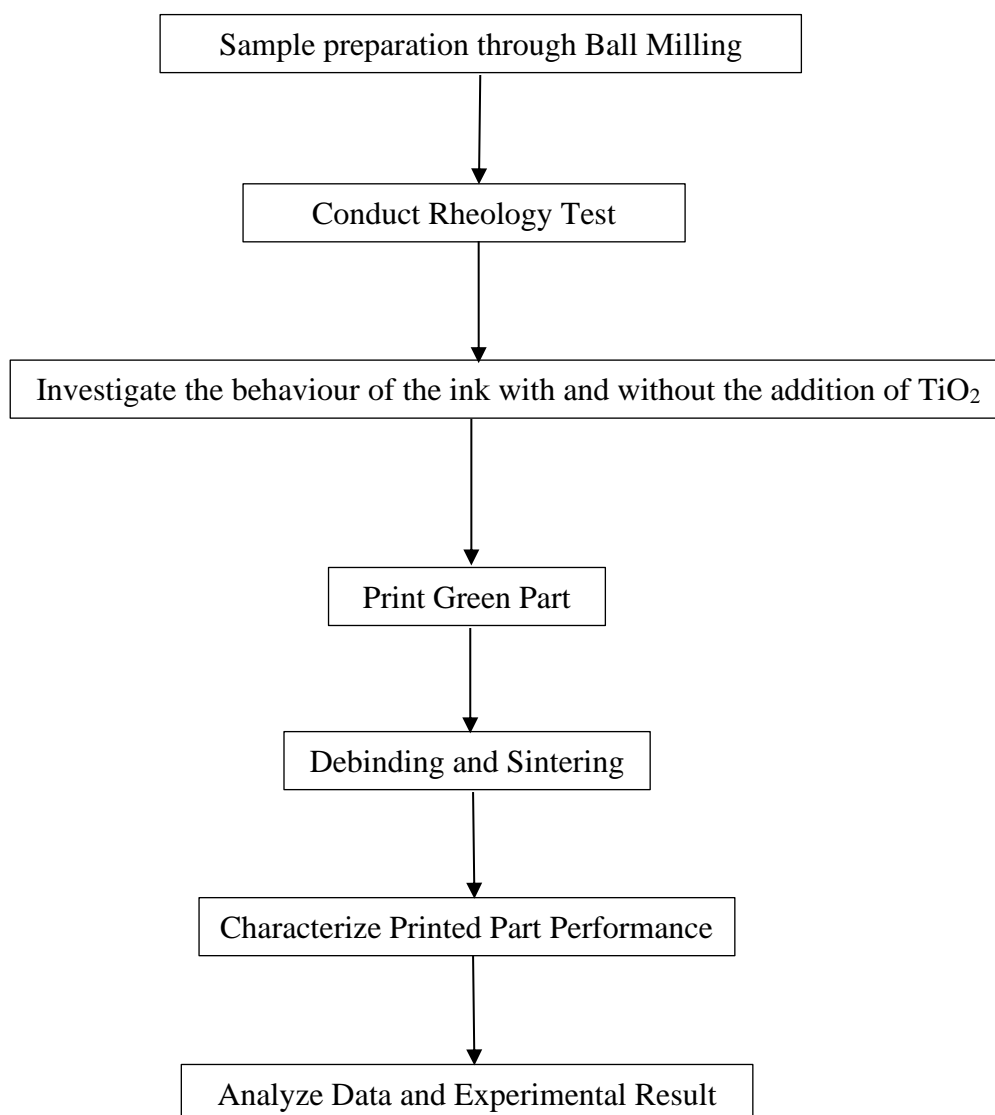


Figure 3.1: Workflow of the project.

3.3 Ink Preparation

For the raw material, alumina powder, it was doped with TiO_2 through ball milling using the roller machine beforehand as shown in Figure 3.2. The range of the formulation of the ink is very important as it will affect the rheological properties of the ink and the printability as well as the shape retention. Firstly cellulose acetate binder was dissolved in acetone. The mixture was sonicated for 5 minutes to ensure the homogeneous mixing as shown in Figure 3.3 (a). Next, it was transferred into the vacuum desiccator for 5 minutes to undergo degas process in order to remove the air bubbles inside the mixture as shown in Figure 3.3 (b). This is because the presence of air bubble could affect the quality

of the printing. Then, it was mixed with alumina powder and loaded into a syringe as shown in Figure 3.4 which loaded to the 3D printer to perform printing.



Figure 3.2: Ball milling for the alumina powder and TiO_2 powder.

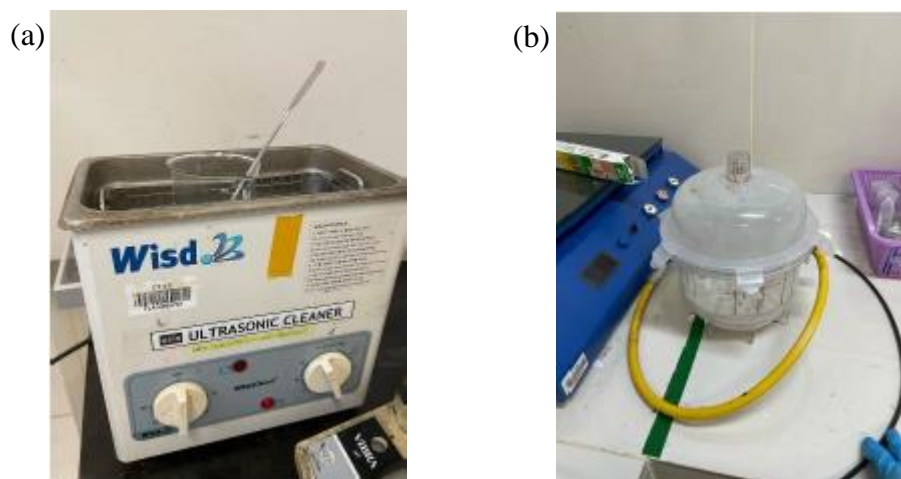


Figure 3.3: Equipment used for ink preparation. (a) Ultrasonic Cleaner. (b) Vacuum Desiccator.

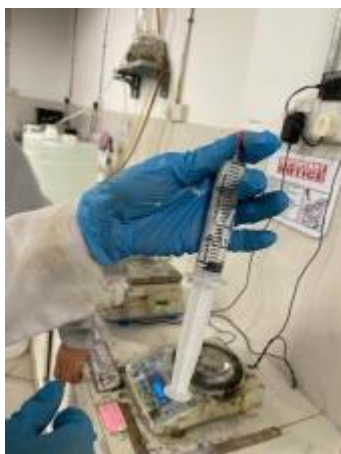


Figure 3.4: Alumina colloidal ink loaded into a syringe.

The alumina content is 40 vol%, and the binder concentration is 100 g/L. Table 3.1 shows the detail of the formulation of the ink:

Table 3.1: Composition of the ink formulation.

Sample	Alumina Content, vol%	Binder Concentration, g/L	Solvent Volume, vol%	Addition of TiO ₂ (wt%)
1	40	100	60	0
2	40	100	60	1

3.3.1 Powder Characteristics

The physical properties of Alumina powder, for example particle size, particle shape and so on were examined via SEM analysis. The micrograph was examined with a magnification of 2000 using 15kV of voltage to identify the particle size of 20 μm . Micrograph will then show the size and shape of the powder, and powder size distribution as well.

3.3.2 Rheology of the ink

Rheology is one of the ways to evaluate the printability of the ink for this Alumina paste in DIW method. The parameters used in this project are the amount of alumina powder and binder. 4 rheological tests have been done in this project to evaluate the rheological properties of the ink such as flow curve, amplitude sweep, frequency sweep, three interval thixotropy (3ITT) test. The flow curve is to identify the relationship between viscosity and shear stress in

different shear rate conditions, shear rate was set between 0.01 s^{-1} to 100 s^{-1} and the curve produced was fitted based on the Hershel-Bulkley model. Amplitude sweep is to obtain the static yield stress of the ink and range of shear strain was set between 0.0001 % and 10 % as well as the constant frequency of 1 Hz and last but not least, frequency sweep is to determine the changes of storage and loss moduli, and damping factor under different range of frequency from 1 to 100 Hz (below yield point) and with a shear stress of 50 Pa. Lastly, 3ITT test is to measure the fast recovery of the elastic behavior of the ink in order to achieve good shape fidelity of the part under constant frequency of 1 Hz, range of shear strain was set between 0.01 % and 1 %, range of interval was set between 120 s and 300 s and range of number was set between 30 and 100 for data points for the 3 intervals in total.

The rheometer plate type used was parallel plate. Torque was recorded on the rotating plate. The alumina paste was placed between the plates and was exerted by capillary forces and hold them in place. The top plate was rotated, shearing the alumina paste and the results were recorded to plot graphs and analyze the trend of different composition of the alumina paste. Figure 3.5 shows the diagram of rheometer with parallel plate system.



Figure 3.5: Diagram of rheometer with parallel plate system.

3.3.3 Slicer software

The slicer software used in this project is PrusaSlicer. Its function is to process the 3D object model, a solid disk with a diameter of 20 mm and a height of 8 mm from the STL file into g-code that is readable by the DIW printer. The slicer split the 3D object model into layers and extrude out by linear movement of

printer extruder. In this slicer software, there are several settings such as print setting, filament setting and printer setting was adjusted, for example, the layer height, first layer height, speed for print move, extrusion multiplier and nozzle diameter to the optimal value. And the specific g-code was read by the DIW printer to print out the green part on platform of the plate. The print setting was set as shown in Table 3.2 below:

Table 3.2: Print setting inside PrusaSlicer.

Setting	Value
Layer height	0.4 mm
First layer height	0.4 mm
Speed for print move	5 mm/s
Extrusion multiplier	1
Nozzle diameter	0.84 mm

3.4 Debinding and Sintering Process

The last two stages of the project are debinding and sintering process. These are the post-printing treatment for the green part generated. For the debinding process, the function is to remove the binder from alumina. Whereas sintering process is to promote interparticle bond within the internal structure. The dimensions before and after both processes were recorded and then compared to make a deduction.

3.4.1 Debinding profile

Debinding is a process where the green part undergoes a binder removal process and becomes a brown part. A LT furnace was used and set to a maximum temperature of 300 °C to thermally degrade the binder that present in the green part. A heating rate of 2 °C/ min was used to heat up the temperature to 300 °C and holding time was about 2 hours. To minimize the residue, debinding has been done in ambient air condition. The green parts were then cooled with cooling rate of -2 °C/ min until the brown part was completely formed. The binder was removed in the form of volatile gas, and the brown part became weak in terms of its structure strength due to the fact the alumina powder was held

loosely apart by the remaining binder and followed up by sintering process. Figure 3.6 illustrates the debinding profile for this project.

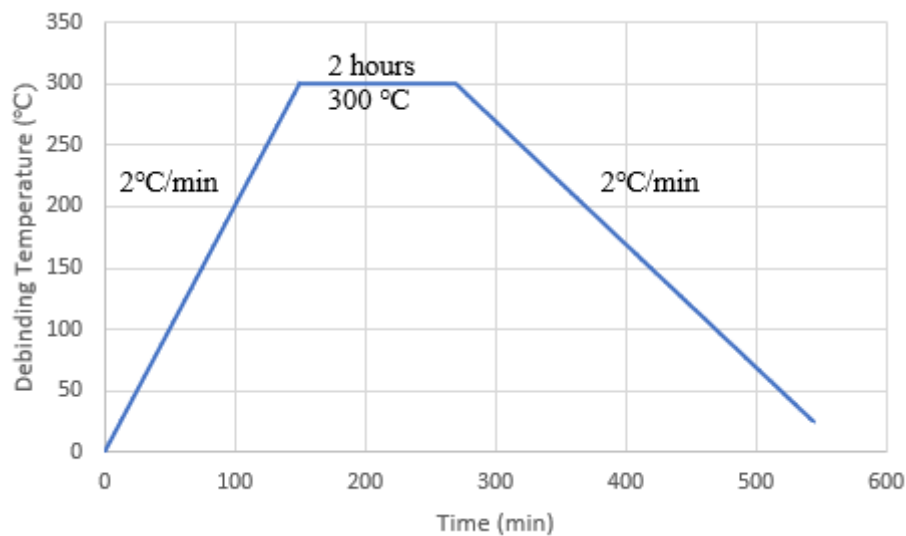


Figure 3.6: Debinding profile for this project.

3.4.2 Sintering profile

Through sintering process, the alumina particle fused together and thus strengthened the interparticle bonding. The remaining binder was removed completely. The whole process here took place in a vacuum furnace with a heating rate of 5 °C/ min to heat up to maximum temperature of 1500 °C and the holding time was about 1 hour. The brown part was then cooled with a cooling rate of -5 °C/ min. Hence, a complete, dense alumina part was obtained. Later on, a series of tests for the characterization of the sintered part were carried out. Figure 3.7 shows the sintering profile for this project.

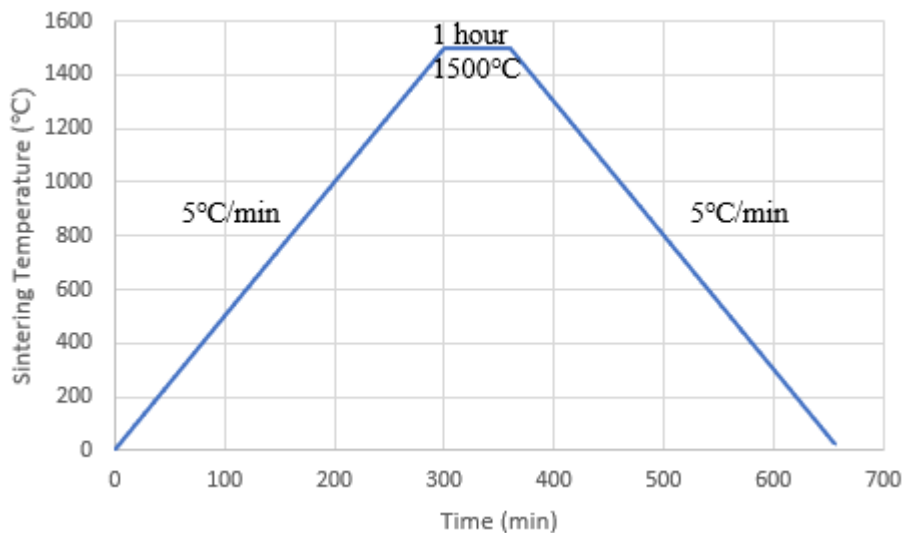


Figure 3.7: Sintering profile for this project.

3.5 Characterization of Sintered Samples

The physical and mechanical properties of the green body and sintered parts were evaluated in this section. There are a few tests carried out as below:

3.5.1 Scanning Electron Microscopy (SEM) Test

Before carrying out this test, the green body or the sintered parts underwent grinding and polishing process to get better surface finish to enhance the effect of the result in this test. Sandpaper was used to grind the surface and polishing process has been done by using the diamond suspension solution. The topological and morphological result of the sample size approximately 20 μm was obtained to evaluate the microstructure behavior of the sintered part. A magnification of 2000 with 15 kV voltage was used throughout this test.

3.5.2 X-Ray Diffraction (XRD) Test

The purpose of this test is to identify the compounds of the sintered part through its crystallinity. A constructive interference monochromatic X-ray was used to generate different diffraction peaks at different angles. In the result, the peak of the compound was determined by matching it with software library database. Surface of the sample was grinded until it is flat to get the crystalline characteristic. The amorphous sample did not have long-ranging order, so it was

unable to clear diffraction peaks as crystalline structure. A scan speed of $2^\circ / \text{min}$ was set and the sample was rotated in the angle between 5° and 85° .

3.5.3 Thermal gravimetric analysis (TGA) Test

The purpose of this test is to study the material's stability and its volatile component by observing the change of the weight of sample against temperature change. It was used to detect evaporation, decomposition, oxidation and other effects of temperature change that leads to the change of the sample mass. For the condition of the test, the atmosphere was purged with nitrogen gas at a rate of 20 ml/min. Next, for the temperature program, the sample was heated from 30°C to 1000°C at a rate of $10^\circ\text{C}/\text{min}$.

3.5.4 Brunauer-Emmett-Teller (BET) Test

The purpose of this test is to determine the surface area per gram of the sample. In BET, the freeze-dried sample was evacuated to expel all the gases and then it was cooled using liquid nitrogen and the degas temperature was set at 150°C .

3.5.5 Vickers Hardness Test

The microhardness of the sintered part is tested using this Vickers Hardness Test. The sintered part was first grinded until it is flat to ensure it is loaded 90° to the contact surface. The hardness tester was adjusted within a range of 5 kgf and 10s of dwells. Next, the Vickers hardness value was recorded based on the depth of the indentation caused by the indentation.

3.5.6 Water Immersion Density Test

The bulk density and volume of porosity of the test specimen were recorded and identified using this test. The amount of air bubble was identified as the porosity have an increasing effect on the buoyant force, reducing the mass of the sample when it is submerged in water. Water immersion measurement kits were used to compare the immersed sample and the dry one. Apparent density and bulk density were evaluated using the Equations 3.1 and 3.2. Theoretical density of alumina as a reference to study the densification of the sample. Then, apparent porosity of the sample was obtained using the density test and a comparison of true and apparent porosity was made. Equation 3.3 was used to evaluate the

volume of porosity of the sample while Equation 3.4 was used to calculate the relative density of the sample. Figure 3.8 shows the diagram of the set up for water immersion density test.



Figure 3.8: Diagram of the set up for water immersion density test (Anderson Materials Evaluation, Inc., n.d.).

Refer to BS EN 1389-2003 standard:

$$\rho_a = \frac{m_1}{m_1 - m_2} \rho_L \quad (3.1)$$

$$\rho_b = \frac{m_1}{m_3 - m_2} \rho_L \quad (3.2)$$

$$V_{\text{pore}} = \frac{m_3 - m_1}{m_3 - m_2} \times 100\% \quad (3.3)$$

$$\rho_{\text{relative}} = \frac{\rho_b}{\rho_{\text{theoretical}}} \times 100\% \quad (3.4)$$

Where,

ρ_a = Apparent density of test specimen in g/cm^3

ρ_b = Bulk density of test specimen in g/cm^3

ρ_{relative} = Relative Density of test specimen in g/cm^3

$\rho_{theoretical}$ = Theoretical Density of the test specimen in g/cm^3

m_1 = Mass of dry test specimen in g

m_2 = Apparent mass of immersed test specimen in g

m_3 = Mass of soaked test specimen in g

ρ_L = Bulk density of liquid (distilled water)

V_{pore} = Volume of porosity in %

3.6 Analysis of alumina powder size

The powder particle was examined using scanning electron microscopy (SEM). Pictures were taken during the process to analyze the powder size via MATLAB as seen in Figure 3.9.

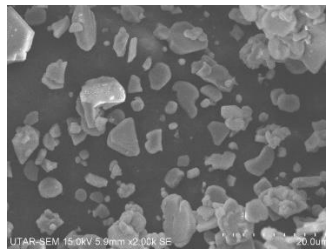


Figure 3.9: Sample to picture of alumina powder particle.

Those pictures were converted to black and white format via MATLAB code as shown in Figure 3.10 and Figure 3.11.

```

Editor - C:\Users\Admin\Desktop\FYP MATLAB\Jillian Wee Rui Ying\Convert_RGB_To_BlackAndWhite.m
Powder_Size_Distribution.m  Convert_RGB_To_BlackAndWhite.m  GSD.m  +
1
2  Ig = im2double(imread('alumina powder sem_m032.tif'));
3  level = 0.40;
4  B1 = im2bw(Ig,level);
5
6  %figure
7  imshow(B1);
8
9  imwrite(B1, 'bwalumina powder sem_m032.tif')
10

```

Figure 3.10: MATLAB code for the conversion of the picture of alumina powder particle.

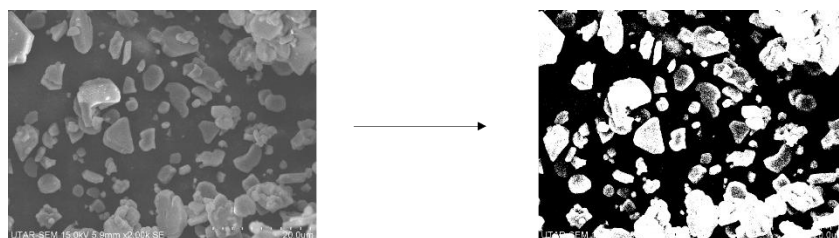


Figure 3.11: Conversion to Black and white version via MATLAB code.

Next, Grain size distribution of alumina powder were analyzed using another MATLAB code.

```
Resolution=0.0493;
Bins=20; % This is
```

Resolution was set at a value of 0.0493 for all the pictures taken and the value was evaluated using the Equation 3.5 below:

$$\text{Resolution} = \frac{\text{Micron}}{\text{Pixel}} \quad (3.5)$$

$$\text{Resolution} = \frac{20}{406}$$

$$= 0.0493$$

In the MATLAB code, these following steps were carried out:

- 1) The R value, radius in each picture indicating the calculated grain size for alumina powder were grouped together and arranged in ascending order in excel.
- 2) Next, the average grain size of the particles were calculated using by excel using the Equation 3.6 below:

$$\text{Average size of particle} = \frac{\text{Total particle size}}{\text{Total number of particle}} \quad (3.6)$$

- 3) Lastly, the particle size distribution curves were plotted to indicate the categories of D10, D50 and D90.

3.7 Summary

In a summary, this chapter 3 consist of the overall workflow of this project, procedures for different ink formulations, 4 rheology tests such as flow curve, amplitude sweep, frequency sweep, and 3ITT test were performed, debinding and sintering detail profiles and lastly 6 tests for the characterization of the sintered sample such as SEM, XRD, TGA, BET, Vickers Hardness Test, Water Immersion Density Test as well as Analysis of alumina powder size were carried out.

CHAPTER 4

RESULTS AND DISCUSSION

4.1 Particle Size Distribution Result

Figure 4.1 and Figure 4.2 show the particle size distribution curve for pure alumina powder. The raw data of the particle diameter was arranged in ascending order and then the categories of D10, D50 and D90 were evaluated by finding the 10th, 50th and 90th of the arranged data.

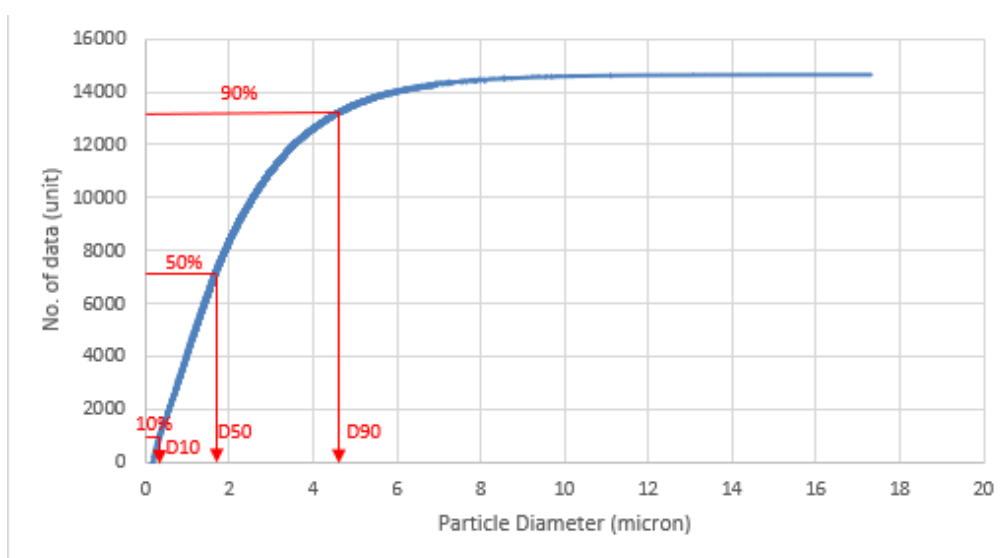


Figure 4.1: Particle size distribution for pure alumina powder.

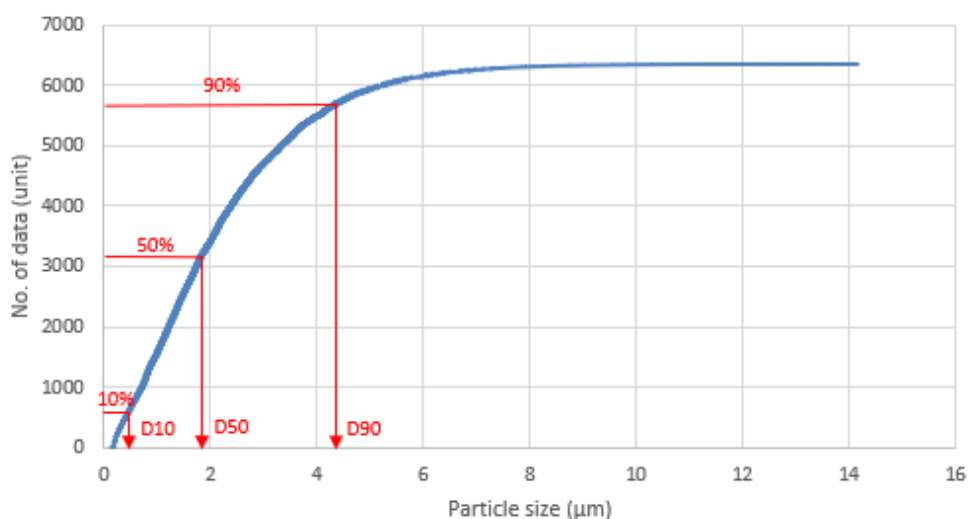


Figure 4.2: Particle size distribution for 1 wt% TiO₂ doped alumina powder.

From Table 4.1 below, regarding the pure alumina powder, it is found that D10 is 0.438735 μm which means 10% of the particles having a diameter less than 0.438735 μm and 90% of the particles having a diameter larger than 0.438735 μm . Next, D50 and D90 is found to be 1.715577 μm and 4.569058 μm respectively. Lastly the average particle size is found to be 2.205119 μm . Through BET analysis, the powder surface area per gram was found to be 1.2968 m^2/g .

Whereas, for the 1 wt% TiO_2 doped alumina powder, it is found that out of the particle size of the powder, D10 is 0.495245 μm which means 10% of the particles having a diameter less than 0.495245 μm and 90% of the particles having a diameter larger than 0.495245 μm . Next, D50 and D90 is found to be 1.84548 μm and 4.407469 μm respectively. Lastly the average particle size is found to be 2.235637 μm . Through BET analysis, the powder surface area per gram was found to be 1.7971 m^2/g .

Table 4.1: Particle size distribution result for pure alumina powder and 1 wt% TiO_2 doped alumina powder.

Samples	D10 (μm)	D50 (μm)	D90 (μm)	Average Particle Size (μm)	BET surface area per gram (m^2/g)
Pure alumina powder	0.438735	1.715577	4.569058	2.205119	1.2968
1 wt% TiO_2 doped alumina powder	0.495245	1.84548	4.407469	2.235637	1.7971

It is observed that the addition of TiO_2 powder to alumina powder barely has any effect to the particle size distribution because all the values for

D10, D50, D90 and average particle size is almost the same. For the surface area per gram, it is noticed that the surface area per gram for the 1 wt% TiO₂ doped alumina powder is larger, this is because the TiO₂ powder is way smaller in size compared to the pure alumina powder, therefore, for the 1 wt% TiO₂ doped alumina powder, TiO₂ help to increase the surface area per gram value.

4.2 Rheological Test Result

Figure 4.3 shows the viscosity and shear stress are measured as a function of shear rate. It is observed in Figure 4.3 (a) and Figure 4.3 (b), both pure alumina powder and 1wt% TiO₂ doped alumina ink result showed the viscosity decreases when the shear rate increases. But for the pure alumina ink, the shear stress decreases slightly when the shear rate increase (ideally shear stress should be increased when shear rate increase). Whereas for 1wt% TiO₂ doped alumina ink, the shear rate behave correctly as the shear stress increases slightly when shear rate increase.

For shear stress, it is important and relatable to printing quality when the minimum force is needed by the 3D printer to extrude the alumina paste. When shear stress is too high, this will lead to clogging in the nozzle, and affect the printing quality. Whereas for viscosity, it is an indication of how well the ink can be extruded and how good the green part can maintain its shape after extrusion. Lastly, shear rate determines how fast the alumina paste is sheared or deformed. If shear rate is too low, this can lead to low printing speeds and low resolution of the printed green part. On the other hand, when it is too high, excessive deformation of the struction or cracking will form.

From these 2 graph, it can be noticed that the addition of TiO₂ barely affect the rheological property of the ink especially for the Shear Stress & Viscosity VS Shear Rate curve.

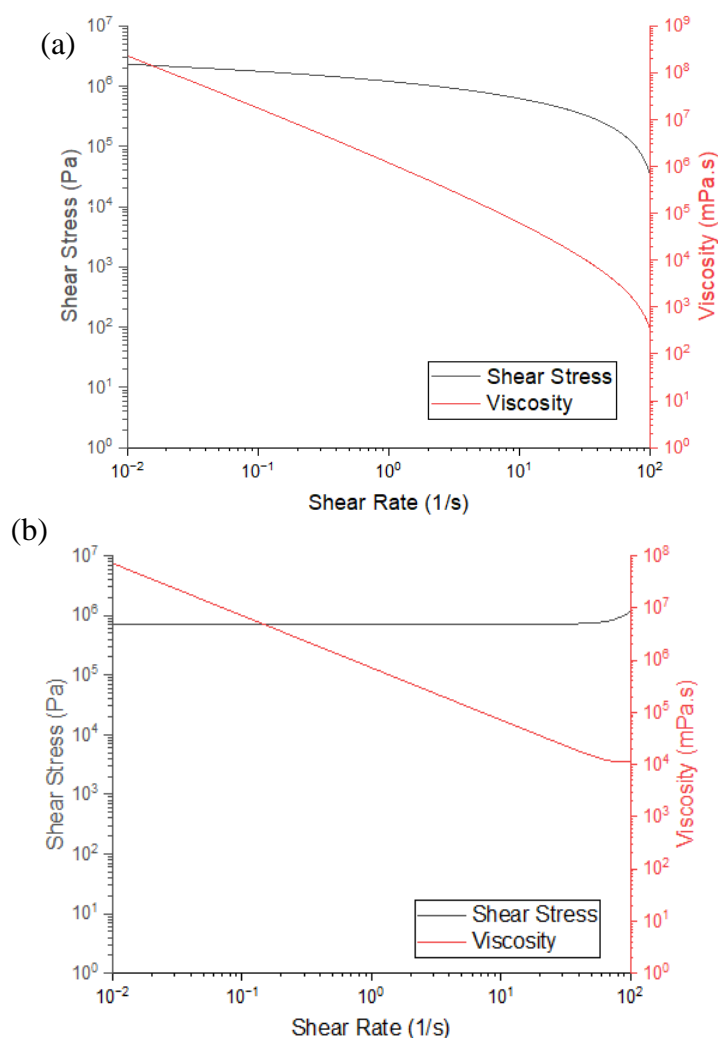


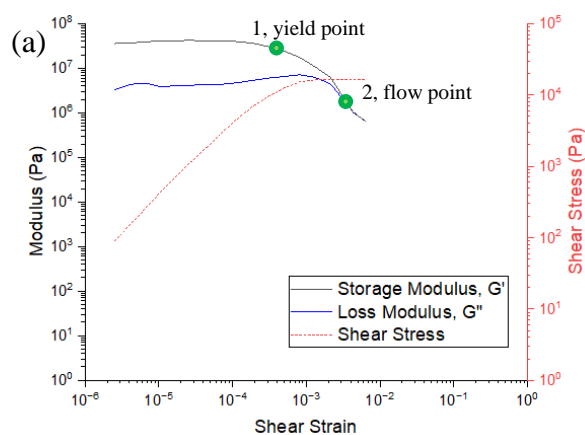
Figure 4.3: Flow curve result for the samples: (a) pure alumina ink. (b) 1wt% TiO_2 doped alumina ink.

Figure 4.4 shows the storage and loss moduli as well as shear stress are measured as a function of shear strain. It is observed that three zone can be distinguished. First zone is called linear viscoelastic region (LVR), in this region, storage modulus, G' is still constant but larger than loss modulus, G'' in overall. For the shear stress, it increases linearly with shear rate. Point 1 is known as yield point. In second region between point 1 and point 2, it can be seen that $G' > G''$ the elastic behavior dominates over the viscous behavior, but the yield stress has been overcome, which means this is an irreversible deformation with solid-like behavior. Point 2 is known as flow point, when $G' = G''$, this is where the transition from elastic behavior to viscous behavior occurs. In third region after point 2, $G'' > G'$, which means the material flow is because of the progressive

breakage and ordering of the internal structure, so the viscos behavior dominates over the elastic behavior.

For storage modulus, it is important and has a indirect relationship with printing quality. It is the energy stored inside a material when the material is deformed and released. A high storage modulus is needed to achieve good shape retention after extrusion. Whereas for loss modulus, it is the energy dissipated as heat when the material is deformed and released. A low loss modulus is desired because it means that the ink has a low viscosity so the ink can flow easily through nozzle during extrusion, therefore smooth surface and uniform dimension of the green part can be produced. Lastly, shear strain could affect indicates the shape retention ability of the ink and how well the ink able to adhere to the previously deposited layers. Too high will collapse the printed structure and too low will lead to poor adhesion between each layers.

From these 2 graph, it can be noticed that the addition of TiO_2 barely affect the rheological property of the ink especially for the G' & G'' & Shear Stress VS Shear Strain curve.



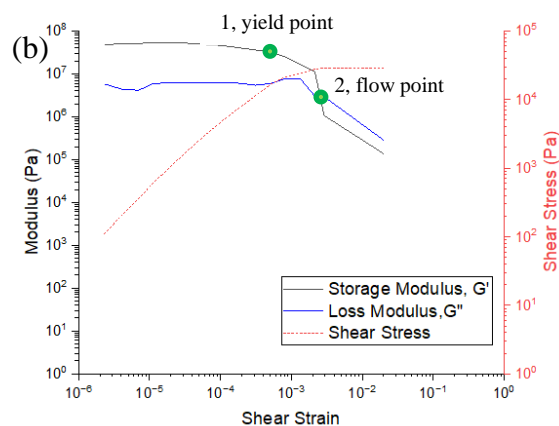


Figure 4.4: Amplitude Sweep result for the samples: (a) pure alumina ink. (b) 1wt% TiO₂ doped alumina ink.

Figure 4.5 shows the storage and loss moduli are measured as a function of frequency. It is observed that the storage modulus, G' dominates over the loss modulus, G'' , indicating that both pure alumina ink and 1 wt% TiO₂ doped alumina ink are in the form of gel-like. Since G' is always over G'' consistently, it indicates that the frequency has no effect on the G' and G'' .

For frequency, it is important and relatable to printing quality. It will affect how the alumina ink respond to the deformation and how the ink flows through the nozzle during extrusion. At low frequency, the ink behaves more like a solid and has higher storage modulus, so it has good shape retentionability. But when frequency is high, the ink behaves like a liquid and has lower storage modulus, so the ink can flow easily through the nozzle during extrusion.

From these 2 graphs, it can be noticed that addition of TiO₂ barely affects the rheological property of the ink especially for the G' & G'' VS Frequency curve.

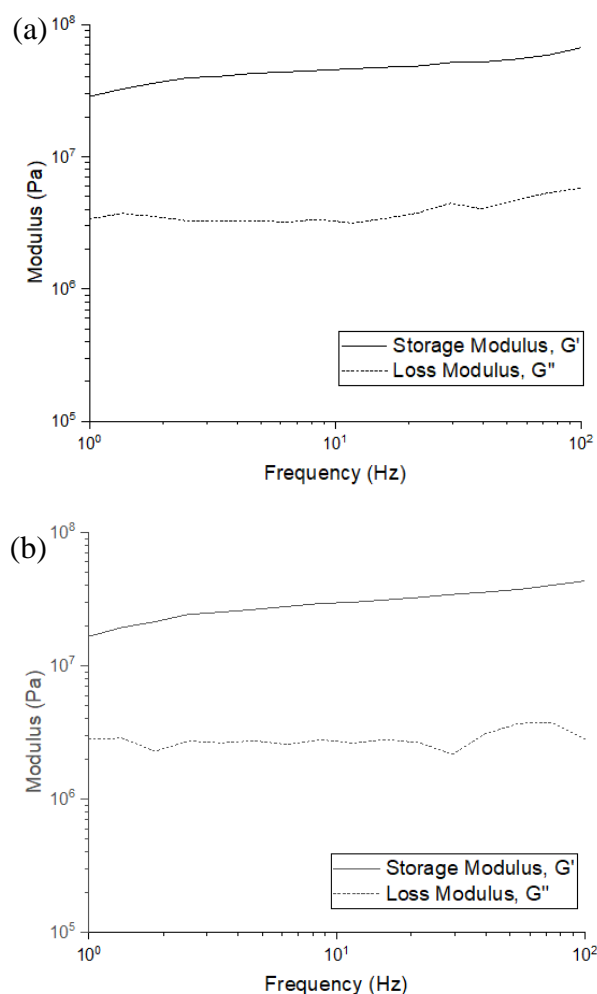


Figure 4.5: Frequency Sweep result for the samples: (a) pure alumina ink. (b) 1wt% TiO_2 doped alumina ink.

Figure 4.6 shows the storage and loss moduli are measured as a function of time. It is observed that there are 3 intervals from the graph. In the first interval, it showed a solid-like behavior ($G' > G''$). However, there is no transition from solid-like behavior to liquid-like behavior in the second interval (Ideally, it should be liquid-like behavior in the second interval) this is due to the long process in 3ITT test and the volatile behavior of acetone. Lastly, the third interval exhibits a solid-like behavior ($G' > G''$) in the third interval.

For time parameter, also important and has an indirect relationship with the printing quality. Since 3ITT test measures the ink's ability to recover its original viscosity and shape after being subjected to shear stress. Thus, an appropriate time interval selected can ensure the alumina ink has a good thixotropic behavior and maintain the shape of the green part after extrusion.

From these 2 graph, it can be noticed that addition of TiO_2 barely affect the rheological property of the ink especially for the G' & G'' VS Time curve.

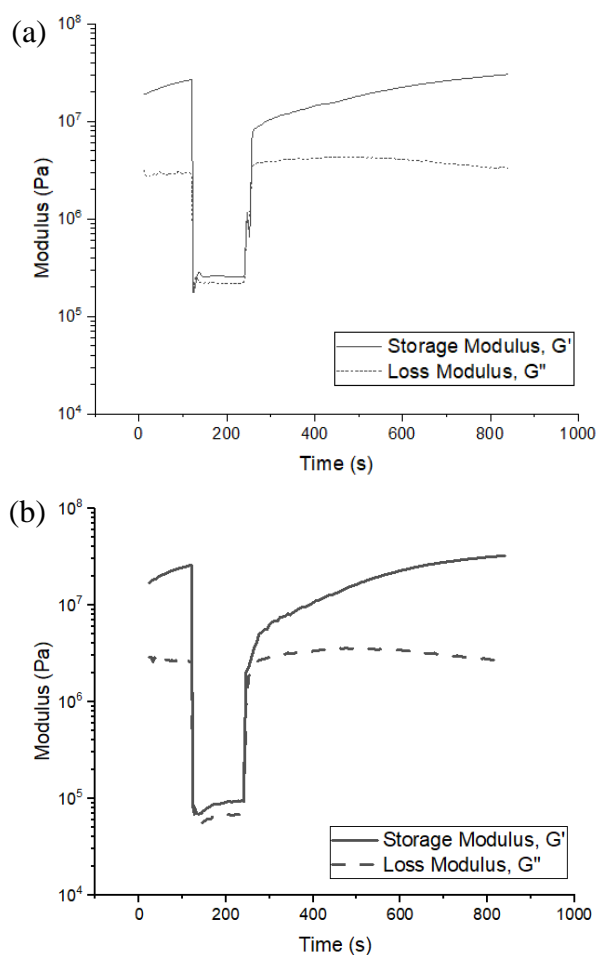


Figure 4.6: 3ITT test result for the samples: (a) pure alumina ink. (b) 1wt% TiO_2 doped alumina ink.

4.3 Printing Result

Figure 4.7 and Figure 4.8 show that the printing of alumina content of 40 vol% and binder concentration of 100 g/L for pure alumina solid disk green parts and 1 wt% TiO_2 doped alumina solid disk green parts respectively. The printed structure is a solid disk with a diameter of 20 mm and a height of 8 mm.

From Figure 4.7, it was found that the pure alumina green part sample 2 is having the best printing result among the samples.

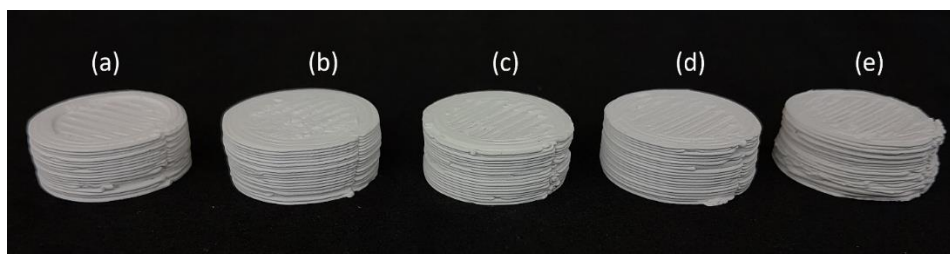


Figure 4.7: Printing result of pure alumina green part with 40 vol% alumina content, 100 g/L binder concentration: (a) Sample 1. (b) Sample 2. (c) Sample 3. (d) Sample 4. (e) Sample 5.

From Figure 4.8, it was found that the 1 wt% TiO₂ doped alumina green part sample 4 is having the best printing result among the samples.

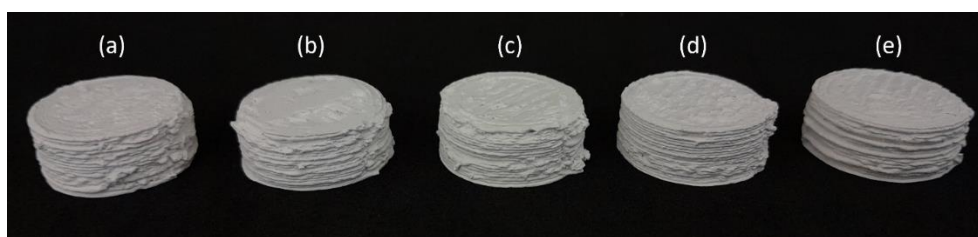


Figure 4.8: Printing result of 1 wt% TiO₂ doped alumina green part with 40 vol% alumina content, 100 g/L binder concentration: (a) Sample 1. (b) Sample 2. (c) Sample 3. (d) Sample 4. (e) Sample 5.

4.4 TGA Result

TGA test is carried out to identify the degradation temperature and get rid of the binder. The TGA result of pure alumina green sample is shown in Figure 4.9, a 2-step thermal degradation curve can be observed. The sample starts to decompose at 200°C and slowly reaching thermal stable level where there is no change in the mass at 400°C. Therefore, debinding temperature is set at 300°C and hold it for 2 hours. Next, it can be observed that the weight percent reached the highest rate of weight loss at 420°C for the first step. For the second step, the binder continues to decompose slowly at 980°C.

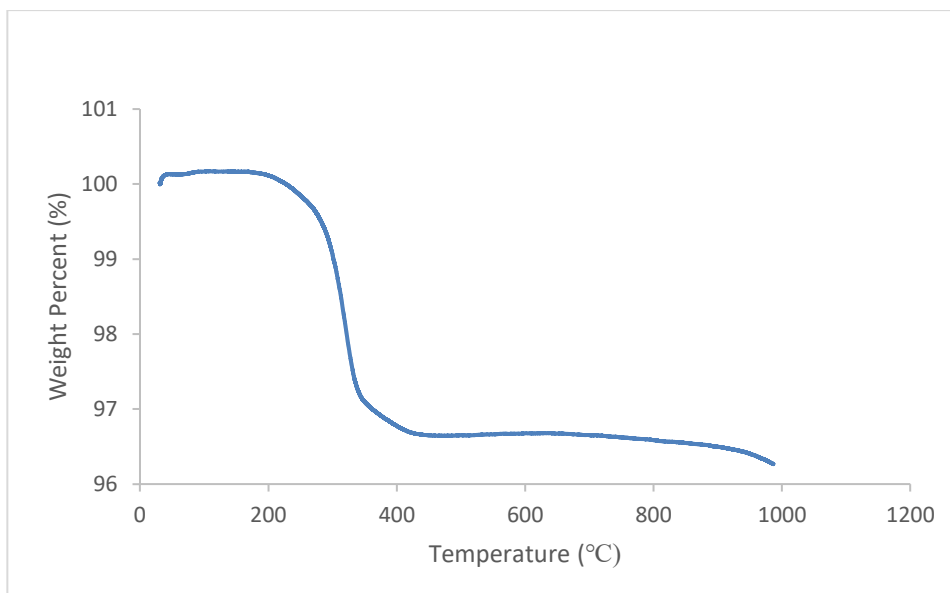


Figure 4.9: Weight percent versus temperature curve for pure alumina scrap (green part).

4.5 SEM Result

SEM image at 2k magnification in Figure 4.10 (a) and Figure 4.10 (b) show irregular shape of the pure alumina powder and 1wt% TiO_2 doped alumina powder respectively. Next, Figure 4.10 (c) and Figure 4.10 (d) show the SEM images of pure alumina solid disk at 2k and 700 magnification respectively. And lastly, Figure 4.10 (e) and Figure 4.10 (f) show the SEM images of 1wt% TiO_2 doped alumina solid disk at 2k and 700 magnification. From the result, to compare pure alumina powder and pure alumina solid disk, it can be noticed that the particle is more compact in solid disk. This is because the binder that bind all the alumina particles together during the mixing of the ink as well as the sintering also help to reduce porosity between particles.

Another thing that can be taken note is that for the powder and solid disk comparison, it is found that there are lesser pores found in 1 wt% TiO_2 doped alumina powder and 1 wt% TiO_2 doped alumina solid disk when compared to the pure alumina powder and pure alumina solid disk. This is because the TiO_2 particles are way smaller than alumina particles, thus it can fill in the spaces between alumina particle, this is proven from the water density test as the volumetric pore percentage for 1 wt% TiO_2 doped alumina solid disk is way smaller compared to the pure solid disk. The addition of TiO_2 to alumina

powder is definitely looked more compact as TiO_2 particles able to occupy those spaces between alumina particles which can be seen in Figure 4.10 below.

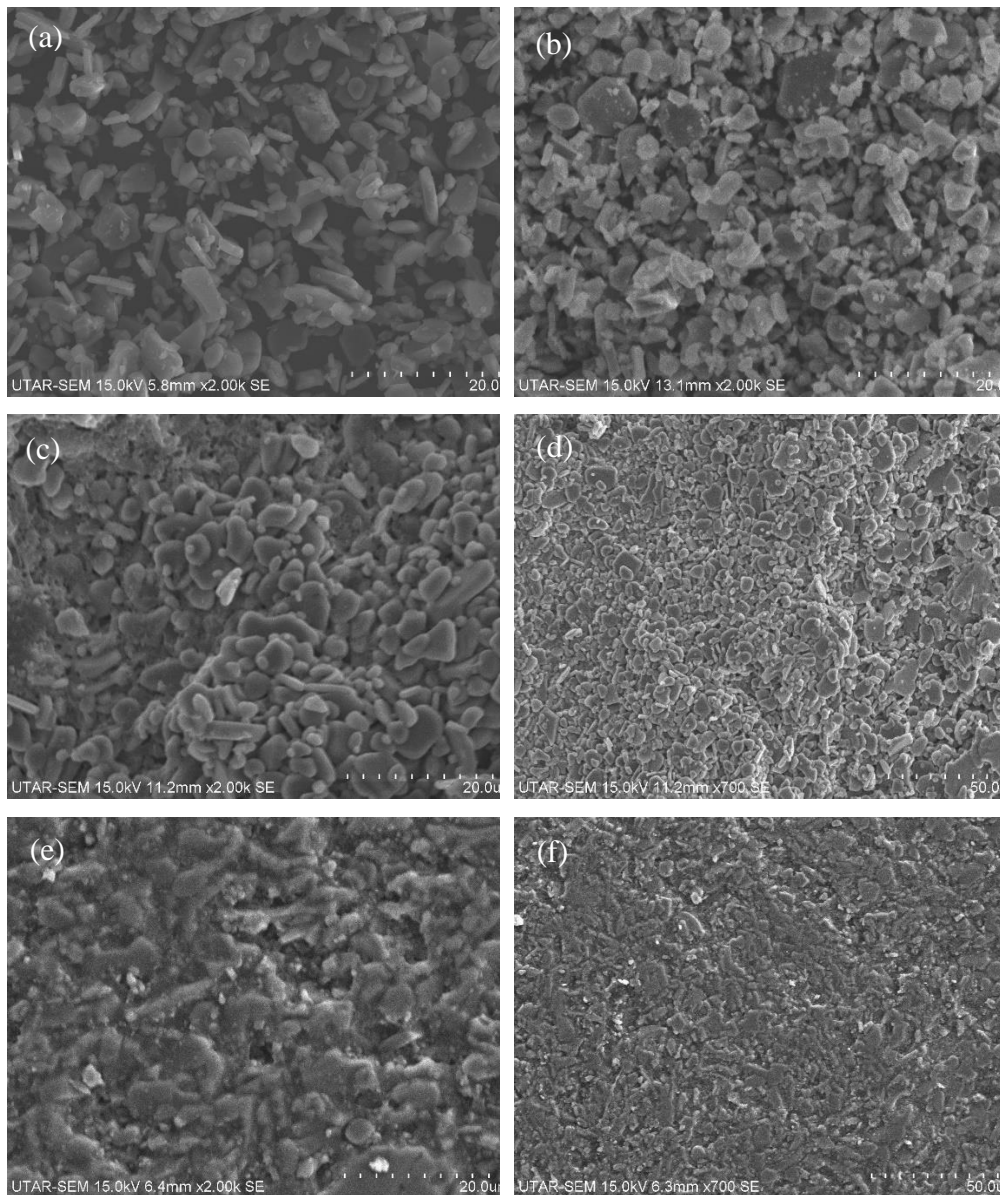


Figure 4.10: SEM result for the samples: (a) pure alumina powder under 2k magnification (b) 1 wt% TiO_2 doped alumina powder under 2k magnification. (c) pure alumina solid disk under 2k magnification. (d) pure alumina solid disk under 700 magnification. (e) 1wt% TiO_2 doped alumina solid disk under 2k magnification (f) 1wt % TiO_2 doped alumina solid disk under 700 magdnification.

4.6 XRD Result

Figure 4.11 shows that all the samples having the same peak pattern. This indicates that there is no any miscellaneous phase or distortion in the structure during sintering process. At peak 43.5° and 57.5° , the intensity counts for pure alumina powder and pure alumina solid disk are higher compared to 1 wt% TiO_2 doped alumina powder and 1 wt% TiO_2 doped alumina solid disk.

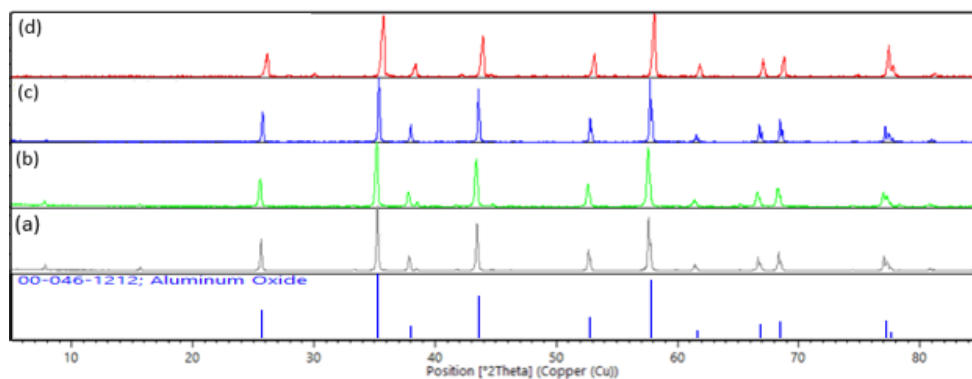


Figure 4.11: XRD peak pattern comparison between the samples: (a) pure alumina powder. (b) 1 wt% TiO_2 doped alumina powder. (c) pure alumina solid disk. (d) 1 wt% TiO_2 doped alumina solid disk.

4.7 Volume Shrinkage

Volume shrinkage means that how much difference in terms of the volume of the sintered samples when compare to its theoretical volume.

Figure 4.12 illustrates the comparison between pure alumina solid disk and 1 wt% TiO_2 doped alumina solid disk, it can be clearly seen that the addition of TiO_2 will increase the volume shrinkage which is not a good sign as the size and appearance of the printed sample is far away different from the design.

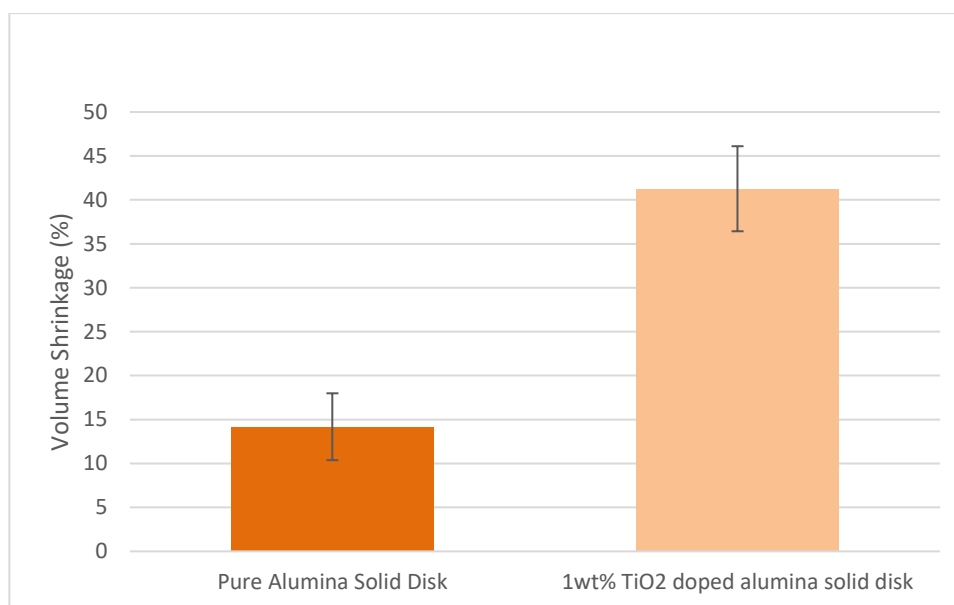


Figure 4.12: Volume Shrinkage comparison between pure alumina solid disk and 1 wt% TiO₂ doped alumina solid disk.

Similar observation was found in a research conducted by Suhasinee and Bhattacharyya (2020). They also found out that the addition of 1 wt % TiO₂ and 1wt% MgO able to increase the percentage of volume shrinkage to 46% - 47% in their doped sintered sample whereas a volume shrinkage of 42% was obtained in the absence of any additive.

4.8 Water Immersion Density Test Result

Relative density here means that the density of the tested samples with respect to its theoretical density. So in this case, the relative density is obtained from the bulk density of the solid disk samples with respect to their theoretical density respectively.

Figure 4.13 shows the comparison between pure alumina solid disk and 1 wt% TiO₂ doped alumina solid disk, it can be clearly seen that the addition of TiO₂ will increase the relative density which is a good sign as it helps to improve the printing quality due to the good sintering effect it gets as the pore is greatly reduced as the TiO₂ particles able to fill the spaces between the existing alumina particles due to the smaller size of TiO₂ particles. Not only that, the effect of sintering of printed sample can also be improved due to the dopant, TiO₂.

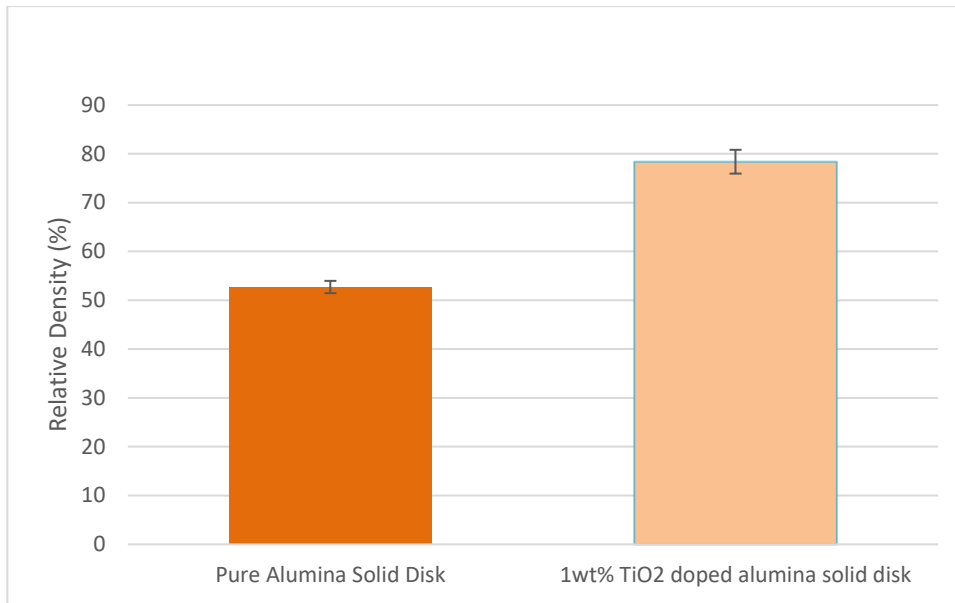


Figure 4.13: Relative Density Comparison between pure alumina solid disk and 1 wt% TiO₂ doped alumina solid disk.

Similar observation was found in a research conducted by Wang and Huang (2008). They also found out that the addition of TiO₂ able to achieve high densification on their tested samples, ultrafine alumina while lowering down the sintering temperature from 1450 °C to 1350 °C.

4.9 Vickers Hardness Test Result

The hardness value for the samples, pure alumina solid disk and 1 wt% TiO₂ doped alumina solid disk are measured and tabulated in the table below. It is noted that the theoretical hardness value of alumina is 780.40 HV.

Figure 4.14 shows the hardness value comparison between pure alumina solid disk and 1 wt% TiO₂ doped alumina solid disk. It is noticed that

there is a huge difference between them. Thus, the addition of TiO_2 definitely help to strengthen the sintered samples which is a positive result to our research.

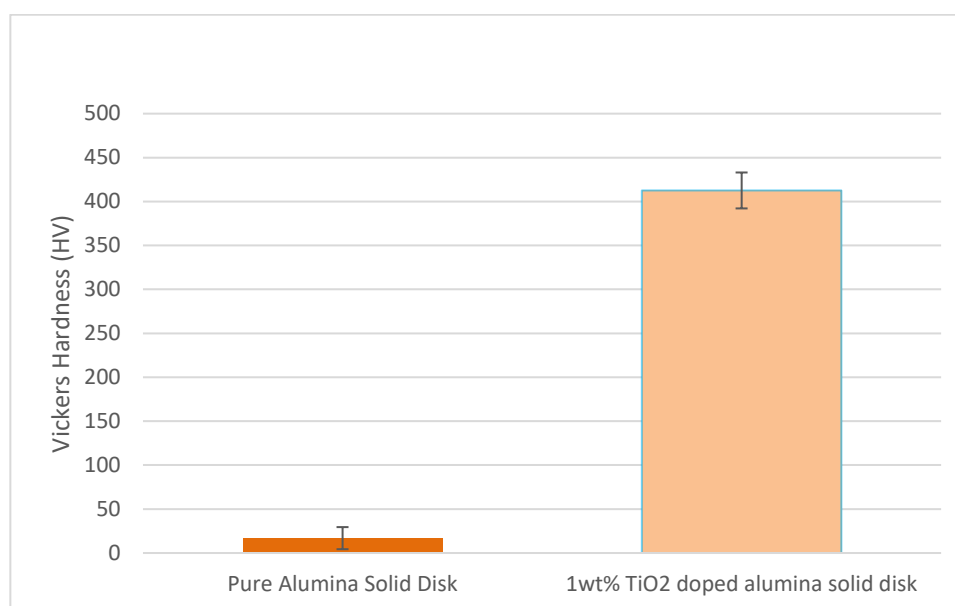


Figure 4.14: Vickers Hardness value comparison between pure alumina solid disk and 1 wt% TiO_2 doped alumina solid disk.

But in overall, both results are not falling within the acceptable range based on the theoretical value as it should be around 780.40 HV. The major reason results in this low Vickers hardness value are because of the high intensity of porosity exist within the sample solid. The porosity will become a stress concentrator that will deteriorate the mechanical properties of the sample such as hardness. Comparatively, the 1 wt% TiO_2 doped alumina solid disk has a Vickers hardness value closer to desired alumina's hardness value, indicating that the addition of TiO_2 to alumina has greatly increased the strength of the sintered samples.

Similar observation was found in a research conducted by Manshor et al. (2015). They also found out that the addition of TiO_2 from 1 wt% to 3wt% able to increase the hardness value from 1516 HV to 1616 HV respectively. The improvement in terms of hardness value of their samples is approximately 6.6 %. Therefore the addition of 1 wt of TiO_2 in this project is supported by the above study as the existence of TiO_2 increased the hardness of the sintered sample.

CHAPTER 5

CONCLUSIONS AND RECOMMENDATIONS

5.1 Conclusions

In conclusion, there are many alumina ceramic 3D technique with the addition of TiO_2 currently in the market, but not yet adopting this DIW technique. There are few advantages of using DIW throughout the project

First of all, the ink used in DIW is the ceramics slurry, due to its viscoelastic behavior, it provides a shape retention ability to the green part, therefore freestanding structure can be printed and it advantageous compared to other technique where support is needed while printing. Secondly, DIW is a simple, and less expensive technique which does not require any involvement of laser or electron beam but able to have similar function as other method which is complex geometry able to be printed out with less defects. Lastly, DIW can operate under room temperature which avoids the printed parts from experiencing thermal and residue stresses.

Our project aimed to study the effect of TiO_2 especially on the rheological properties of alumina ink as well as the sinterability of the sintered samples via DIW method. The rheological properties were evaluated through rheological tests such as flow curve, amplitude sweep, and frequency sweep, and 3ITT test. While for the sinterability, it was examined through several characterization test such as SEM, XRD, TGA, BET, Vickers Hardness Test as well as Water Immersion Density Test.

From the result obtained, it was found that the addition of TiO_2 helped to improve the morphology of the alumina feedstock. It can be seen from the SEM result that there were lesser pore found in doped alumina powder and doped alumina solid disk. Next, TiO_2 was proven that it barely affect the particle size distribution of categories of D10, D50 and D90 as well as the average particle size. Next it can be noticed that both the pure and doped alumina ink displayed almost the same rheological behavior, therefore it can be said that the addition of TiO_2 barely affect the rheological properties of the alumina ink. But for the surface area per gram, it is observed that the 1 wt% TiO_2 doped alumina

powder is larger due to the smaller size of TiO_2 powder additives. For the printing result, the addition of TiO_2 powder barely affect the printing quality and appearance of the green parts. In XRD, there is no difference between the pure alumina powders and 1 wt% TiO_2 doped alumina powders as well as those solid disks as the result showed that all of them having the same peak pattern. Furthermore, the addition of TiO_2 to the raw material, alumina powder increased the volume shrinkage which posts a negative printing effect to the sintered samples. But, it helped to increase the relative density of the sintered samples therefore the sintering effect and the quality of the sintered samples can be improved. Lastly, the addition of TiO_2 increases the Vickers hardness value of the sintered object by a lot which is a good sign in terms of the printing stability.

5.2 Recommendations for future work

The results show that the densification of the samples is limited by the porosity exists inside the samples. Although TiO_2 helped to reduce the porosity of the samples, but to further reduce it, careful handling in the preparation of the sample must be done especially in the vacuum desiccator equipment. There are sometimes leaks in the connection points, so make sure there is no leakage during the operation. To make sure that all the bubble is removed completed, the period can be extended longer till 7 minutes. Not only that, porosity might come from the printing parameter, so it should fine tune in order to get the optimal parameters.

For the printing quality, it can be improved by conducting linear advanced analysis to predict the pressure build-up in the extruder at high printing speed condition. Therefore, from the prediction, we can reduce the amount of the ink extruded just before nozzle stops or change direction. Thus the blobs will less likely to appear in the sharp corner of the samples. Next, since all the printed sample is in simple shape and size, I would like to suggest for the future work is that, the weight percent of TiO_2 could goes higher for example 1.5 wt% , 2 wt%, and 2.5wt% and so on.

Next, the size of the green part could go higher and bigger to see whether the 3D printing of alumina can support larger object although there are many other factors to be considered. Moreover, to examine the robustness of the

printing, one of the aspect is the complexity of the printed sample, I would like to suggest to print a lattice structure to see how stable the object can be especially its self-supporting capability and also the shape retention ability.

Last but not least, manipulating the sintering temperature to see the result of the sintered part especially their performance on the characterisation tests by increasing the sintering temperature to 1600 °C. Lastly, since the alumina shaped used in this project is non-spherical, so I would like to recommend to examine the behaviour of the spherical-shaped alumina powder especially the physical and machinal properties of the sintered parts.

REFERENCES

- Additive Manufacturing Research Group, n.d. About Additive Manufacturing. *Powder Bed Fusion*, [online] Available at: <<https://www.lboro.ac.uk/research/amrg/about/the7categoriesofadditivemanufacturing/powderbedfusion/>> [Accessed 15 August 2022].
- Allaire, F., Marple, B.R. and Boulanger, J., 1994. Injection molding of submicrometer zirconia: blend formulation and rheology. *Ceramics International*, [e-journal] 20(5), pp.319–325. [https://doi.org/10.1016/0272-8842\(94\)90049-3](https://doi.org/10.1016/0272-8842(94)90049-3).
- Anderson Materials Evaluation, Inc., n.d. Density and Porosity Measurements of Solid Materials, [online] Available at: <<https://andersonmaterials.com/density-and-porosity-measurements-of-solid-materials/>> [Accessed 10 August 2022].
- Bonada, J., Xuriguera, E., Calvo, L., Poudelet, L., Cardona, R., Padilla, J.A., Niubó, M. and Fenollosa, F., 2019. Analysis of printing parameters for metal additive manufactured parts through Direct Ink Writing process. *Procedia Manufacturing*, [e-journal] 41, pp.666–673. <https://doi.org/10.1016/j.promfg.2019.09.056>.
- Chateau, X., 2012. Particle packing and the rheology of concrete. In: *Understanding the Rheology of Concrete*, [e-journal], pp.117–143. <https://doi.org/10.1533/9780857095282.2.117>.
- Chen, Z., Li, Z., Li, J., Liu, C., Lao, C., Fu, Y., Liu, C., Li, Y., Wang, P. and He, Y., 2019. 3D printing of ceramics: A review. *Journal of the European Ceramic Society*, [e-journal] 39(4), pp.661–687. <https://doi.org/10.1016/j.jeurceramsoc.2018.11.013>.
- Cooke, S., Ahmadi, K., Willerth, S. and Herring, R., 2020. Metal additive manufacturing: Technology, metallurgy and modelling. *Journal of Manufacturing Processes*, [e-journal] 57, pp.978–1003. <https://doi.org/10.1016/j.jmapro.2020.07.025>.
- del-Mazo-Barbara, L. and Ginebra, M.-P., 2021. Rheological characterisation of ceramic inks for 3D direct ink writing: A review. *Journal of the European*

- Ceramic Society*, [e-journal] 41(16), pp.18–33.
<https://doi.org/10.1016/j.jeurceramsoc.2021.08.031>.
- Ding, D., Pan, Z., Cuiuri, D. and Li, H., 2015. Wire-feed additive manufacturing of metal components: technologies, developments and future interests. *The International Journal of Advanced Manufacturing Technology*, [e-journal] 81(1–4), pp.465–481. <https://doi.org/10.1007/s00170-015-7077-3>.
- Enneti, R.K., Onbattuvelli, V.P. and Atre, S.V., 2012. Powder binder formulation and compound manufacture in metal injection molding (MIM). In: *Handbook of Metal Injection Molding*, [e-journal], pp.64–92. <https://doi.org/10.1533/9780857096234.1.64>.
- Feilden, E., Blanca, E.G.-T., Giuliani, F., Saiz, E. and Vandeperre, L., 2016. Robocasting of structural ceramic parts with hydrogel inks. *Journal of the European Ceramic Society*, [e-journal] 36(10), pp.2525–2533. <https://doi.org/10.1016/j.jeurceramsoc.2016.03.001>.
- Frazier, W.E., 2014. Metal Additive Manufacturing: A Review. *Journal of Materials Engineering and Performance*, [e-journal] 23(6), pp.1917–1928. <https://doi.org/10.1007/s11665-014-0958-z>.
- Godwin, A.D., 2000. PLASTICIZERS. In: *Applied Polymer Science: 21st Century*, [e-journal], pp.157–175. <https://doi.org/10.1016/B978-008043417-9/50011-8>.
- Gupta, R.K., Anil Kumar, V. and Khanra, G.P., 2018. Reactive and liquid-phase sintering techniques. In: *Intermetallic Matrix Composites*, [e-journal], pp.303–318. <https://doi.org/10.1016/B978-0-85709-346-2.00011-X>.
- Heaney, D.F., 2012. *Handbook of Metal Injection Molding*, Woodhead Publishing Limited
- Jiang, J., Ni, N., Hao, W., Zhao, X., Guo, F., Fan, X. and Xiao, P., 2019. Effects of sintering atmosphere on the densification and microstructure of yttrium aluminum garnet fibers prepared by sol-gel process. *Journal of the European Ceramic Society*, [e-journal] 39(16), pp.5332–5337. <https://doi.org/10.1016/j.jeurceramsoc.2019.08.033>.
- Kim, B.-N., Hiraga, K., Morita, K. and Yoshida, H., 2009. Effects of heating rate on microstructure and transparency of spark-plasma-sintered alumina.

Journal of the European Ceramic Society, [e-journal] 29(2), pp.323–327.
<https://doi.org/10.1016/j.jeurceramsoc.2008.03.015>.

Li, H., Liu, Y., Liu, Y., Zeng, Q., Hu, K., Lu, Z. and Liang, J., 2020. Effect of sintering temperature in argon atmosphere on microstructure and properties of 3D printed alumina ceramic cores. *Journal of Advanced Ceramics*, [e-journal] 9(2), pp.220–231. <https://doi.org/10.1007/s40145-020-0362-0>.

Li, Y., Li, L. and Khalil, K.A., 2007. Effect of powder loading on metal injection molding stainless steels. *Journal of Materials Processing Technology*, [e-journal] 183(2–3), pp.432–439.
<https://doi.org/10.1016/j.jmatprotec.2006.10.039>.

Li, H., Xi, X., Ma, J., Hua, K. and Shui, A., 2017. Low-temperature sintering of coarse alumina powder compact with sufficient mechanical strength. *Ceramics International*, [e-journal] 43(6), pp.5108–5114.
<https://doi.org/10.1016/j.ceramint.2017.01.024>.

Linke, R., 2017. Additive Manufacturing, explained. *What is additive manufacturing?*, [online] Available at: <<https://mitsloan.mit.edu/ideas-made-to-matter/additive-manufacturing-explained>> [Accessed 10 August 2022].

Liu, J., Li, P., Jin, D., Her, S., Kim, J., Yoon, Y., Baldassari, M., Bae, S., 2023. Evaluation of the mechanical and photocatalytic properties of TiO₂-reinforced cement-based materials in binder jet 3D printing. *Journal of Building Engineering*, [e-journal] 72, p.6017.
<https://doi.org/10.1016/j.jobe.2023.106618>.

Liu, N., Sun, X., Chen, Z., Xu, Z., Dai, N., Shi, G., Cai, S., Lv, X. and Zheng, C., 2022. Direct ink writing of dense alumina ceramics prepared by rapid sintering. *Ceramics International*, [e-journal].
<https://doi.org/10.1016/j.ceramint.2022.07.028>.

Lucena, M. da C.C., v. de Alencar, A.E., Mazzeto, S.E. and Soares, S. de A., 2003. The effect of additives on the thermal degradation of cellulose acetate. *Polymer Degradation and Stability*, [e-journal] 80(1), pp.149–155.
[https://doi.org/10.1016/S0141-3910\(02\)00396-8](https://doi.org/10.1016/S0141-3910(02)00396-8).

M'Barki, A., Bocquet, L. and Stevenson, A., 2017. Linking Rheology and Printability for Dense and Strong Ceramics by Direct Ink Writing. *Scientific Reports*, [e-journal] 7(1), p.6017. <https://doi.org/10.1038/s41598-017-06115-0>.

- Manshor, H., Aris, S. M., Azhar, A. Z. A., Abdullah, E. C., Ahmad, Z. A., 2015. Effects of TiO₂ addition on the phase, mechanical properties, and microstructure of zirconia-toughened alumina ceramic composite. *Ceramics International*. [e-journal] 41(3), pp. 3961-3967. <https://doi.org/10.1016/j.ceramint.2014.11.080>.
- Mostafaei, A., Rodriguez De Vecchis, P., Nettleship, I. and Chmielus, M., 2019. Effect of powder size distribution on densification and microstructural evolution of binder-jet 3D-printed alloy 625. *Materials & Design*, [e-journal] 162, pp.375–383. <https://doi.org/10.1016/j.matdes.2018.11.051>.
- Ngo, T.D., Kashani, A., Imbalzano, G., Nguyen, K.T.Q. and Hui, D., 2018. Additive manufacturing (3D printing): A review of materials, methods, applications and challenges. *Composites Part B: Engineering*, [e-journal] 143, pp.172–196. <https://doi.org/10.1016/j.compositesb.2018.02.012>.
- Pan, Y., Li, H., Liu, Y., Liu, Y., Hu, K., Wang, N., Lu, Z., Liang, J. and He, S., 2020. Effect of Holding Time During Sintering on Microstructure and Properties of 3D Printed Alumina Ceramics. *Frontiers in Materials*, [e-journal] 7. <https://doi.org/10.3389/fmats.2020.00054>.
- Qian, C., Hu, K., Shen, Z., Wang, Q., Li, P., Lu, Z., 2023. Effect of sintering aids on mechanical properties and microstructure of alumina ceramic via stereolithography. *Ceramics International*, [e-journal] 49 (11), pp.17506–17523. <https://doi.org/10.1016/j.ceramint.2023.02.118>.
- Roy, S.K., 1995. Effects of Atmosphere on Sintering of Alumina. *Transactions of the Indian Ceramic Society*, [e-journal] 54(5), pp.190–196. <https://doi.org/10.1080/0371750X.1995.10804718>.
- Rueschhoff, L., Costakis, W., Michie, M., Youngblood, J. and Trice, R., 2016. Additive Manufacturing of Dense Ceramic Parts via Direct Ink Writing of Aqueous Alumina Suspensions. *International Journal of Applied Ceramic Technology*, [e-journal] 13(5), pp.821–830. <https://doi.org/10.1111/ijac.12557>.
- Sahari, J., Sulong, A.B. and Husaini, T., 2016. CRITICAL POWDER LOADING AND RHEOLOGICAL PROPERTIES OF POLYPROPYLENE/GRAPHITE COMPOSITE FEEDSTOCK FOR BIPOLAR PLATE APPLICATION. *Malaysian Journal of Analytical Science*, [e-journal] 20(3), pp.687–696. <https://doi.org/10.17576/mjas-2016-2003-30>.

- Sames, W.J., List, F.A., Pannala, S., Dehoff, R.R. and Babu, S.S., 2016. The metallurgy and processing science of metal additive manufacturing. *International Materials Reviews*, [e-journal] 61(5), pp.315–360. <https://doi.org/10.1080/09506608.2015.1116649>.
- Shahzad, A. and Lazoglu, I., 2021. Direct ink writing (DIW) of structural and functional ceramics: Recent achievements and future challenges. *Composites Part B: Engineering*, [e-journal] 225, p.109249. <https://doi.org/10.1016/j.compositesb.2021.109249>.
- Sing, S.L., Tey, C.F., Tan, J.H.K., Huang, S. and Yeong, W.Y., 2020. 3D printing of metals in rapid prototyping of biomaterials: Techniques in additive manufacturing. In: *Rapid Prototyping of Biomaterials*, [e-journal], pp.17–40. <https://doi.org/10.1016/B978-0-08-102663-2.00002-2>.
- Smay, J.E., Cesarano, J. and Lewis, J.A., 2002. Colloidal Inks for Directed Assembly of 3-D Periodic Structures. *Langmuir*, [e-journal] 18(14), pp.5429–5437. <https://doi.org/10.1021/la0257135>.
- Suhasinee Behera, P. and Bhattacharyya, S. (2020). Sintering and microstructural study of mullite prepared from kaolinite and reactive alumina: Effect of MgO and TiO₂. *International Journal of Applied Ceramic Technology*, [e-journal] 18(1), pp.81–90.
- Supati, R., Loh, N.H., Khor, K.A. and Tor, S.B., 2000. Mixing and characterization of feedstock for powder injection molding. *Materials Letters*, [e-journal] 46(2–3), pp.109–114. [https://doi.org/10.1016/S0167-577X\(00\)00151-8](https://doi.org/10.1016/S0167-577X(00)00151-8).
- Support, A., 2020. Print Parameter Optimization Guide. *Extrusion Test*, [online] Available at: < <https://www.allevi3d.com/print-parameter-optimization/> > [Accessed 11 August 2022].
- Supriadi, S., Suharno, B., Hidayatullah, R., Maulana, G. and Baek, E.R., 2017. Thermal Debinding Process of SS 17-4 PH in Metal Injection Molding Process with Variation of Heating Rates, Temperatures, and Holding Times. *Solid State Phenomena*, [e-journal] 266, pp.238–244. <https://doi.org/10.4028/www.scientific.net/SSP.266.238>.
- Tafti, A.A., Demers, V., Majdi, S.M., Vachon, G. and Brailovski, V., 2021. Effect of Thermal Debinding Conditions on the Sintered Density of Low-

Pressure Powder Injection Molded Iron Parts. *Metals*, [e-journal] 11(2), p.264. <https://doi.org/10.3390/met11020264>.

Ting, C. H., Tan, C. Y., Ramesh, S., Sopyan, I. and Teng, W. D., 2008. Sintering behaviour of TiO₂-doped alumina for biomedical application. In: Lis, S, 4th Kuala Lumpur International Conference on Biomedical Engineering, Kuala Lumpur, Malaysia, January 2008. Kuala Lumpur: Malaysia.

Tubío, C.R., Antelo, J., Guitián, F. and Gil, A., 2018. 3D Printed Composites of Copper–Aluminum Oxides. *3D Printing and Additive Manufacturing*, [e-journal] 5(1), pp.46–52. <https://doi.org/10.1089/3dp.2017.0101>.

Vilaro, T., Colin, C. and Bartout, J.D., 2011. As-Fabricated and Heat-Treated Microstructures of the Ti-6Al-4V Alloy Processed by Selective Laser Melting. *Metallurgical and Materials Transactions A*, [e-journal] 42(10), pp.3190–3199. <https://doi.org/10.1007/s11661-011-0731-y>.

Wang, C.J. and Huang, C.Y., 2008. Effect of TiO₂ addition on the sintering behavior, hardness and fracture toughness of an ultrafine alumina. *Materials Science and Engineering: A*, [e-journal] 492(1-2), pp. 306-310. <https://doi.org/10.1016/j.msea.2008.04.048>.

Wu, H., Cheng, Y., Liu, W., He, R., Zhou, M., Wu, S., Song, X. and Chen, Y., 2016. Effect of the particle size and the debinding process on the density of alumina ceramics fabricated by 3D printing based on stereolithography. *Ceramics International*, [e-journal] 42(15), pp.17290–17294. <https://doi.org/10.1016/j.ceramint.2016.08.024>.

Yan, Z., Hara, S. and Shikazono, N., 2017. Effect of powder morphology on the microstructural characteristics of La_{0.6}Sr_{0.4}Co_{0.2}Fe_{0.8}O₃ cathode: A Kinetic Monte Carlo investigation. *International Journal of Hydrogen Energy*, [e-journal] 42(17), pp.12601–12614. <https://doi.org/10.1016/j.ijhydene.2017.03.136>.

APPENDICES

NIL